

Article

A Molybdenum(VI) Complex of 5-(2-pyridyl-1-oxide)tetrazole: Synthesis, Structure, and Transformation into a MoO₃-Based Hybrid Catalyst for the Epoxidation of Bio-Olefins

Martinique S. Nunes ¹, Diana M. Gomes ¹, Ana C. Gomes ¹, Patrícia Neves ¹, Ricardo F. Mendes ¹,
Filipe A. Almeida Paz ¹, André D. Lopes ^{2,3}, Martyn Pillinger ¹, Anabela A. Valente ^{1,*}
and Isabel S. Gonçalves ^{1,*}

¹ CICECO—Aveiro Institute of Materials, Department of Chemistry, University of Aveiro, Campus Universitário de Santiago, 3810-193 Aveiro, Portugal

² Center of Marine Sciences, CCMAR, Gambelas Campus, University of Algarve (UAlg), 8005-139 Faro, Portugal

³ Department of Chemistry and Pharmacy, Faculty of Sciences and Technology, FCT, Gambelas Campus, University of Algarve (UAlg), 8005-139 Faro, Portugal

* Correspondence: atav@ua.pt (A.A.V.); igoncalves@ua.pt (I.S.G.)

Abstract: The discovery of heterogeneous catalysts synthesized in easy, sustainable ways for the valorization of olefins derived from renewable biomass is attractive from environmental, sustainability, and economic viewpoints. Here, an organic–inorganic hybrid catalyst formulated as [MoO₃(Hpto)]·H₂O (**2**), where Hpto = 5-(2-pyridyl-1-oxide)tetrazole, was prepared by a hydrolysis–condensation reaction of the complex [MoO₂Cl₂(Hpto)]·THF (**1**). The characterization of **1** and **2** by FT-IR and Raman spectroscopies, as well as ¹³C solid-state NMR, suggests that the bidentate N,O-coordination of Hpto in **1** (forming a six-membered chelate ring, confirmed by X-ray crystallography) is maintained in **2**, with the ligand coordinated to a molybdenum oxide substructure. Catalytic studies suggested that **2** is a rare case of a molybdenum oxide/organic hybrid that acts as a stable solid catalyst for olefin epoxidation with *tert*-butyl hydroperoxide. The catalyst was effective for converting biobased olefins, namely fatty acid methyl esters (methyl oleate, methyl linoleate, methyl linolenate, and methyl ricinoleate) and the terpene limonene, leading predominantly to the corresponding epoxide products with yields in the range of 85–100% after 24 h at 70 °C. The versatility of catalyst **2** was shown by its effectiveness for the oxidation of sulfides into sulfoxides and sulfones, at 35 °C (quantitative yield of sulfoxide plus sulfone, at 24 h; sulfone yields in the range of 77–86%). To the best of our knowledge, **2** is the first molybdenum catalyst reported for methyl linolenate epoxidation, and the first of the family [MoO₃(L)_x] studied for methyl ricinoleate epoxidation.

Keywords: dioxomolybdenum (VI) complexes; molybdenum oxide; organic–inorganic hybrid materials; 5-(2-pyridyl-1-oxide)tetrazole; epoxidation; bio-olefins; limonene; FAMES; sulfoxidation



Citation: Nunes, M.S.; Gomes, D.M.; Gomes, A.C.; Neves, P.; Mendes, R.F.; Paz, F.A.A.; Lopes, A.D.; Pillinger, M.; Valente, A.A.; Gonçalves, I.S. A Molybdenum(VI) Complex of 5-(2-pyridyl-1-oxide)tetrazole: Synthesis, Structure, and Transformation into a MoO₃-Based Hybrid Catalyst for the Epoxidation of Bio-Olefins. *Catalysts* **2023**, *13*, 565. <https://doi.org/10.3390/catal13030565>

Academic Editor: Takeshi Ohkuma

Received: 10 February 2023

Revised: 5 March 2023

Accepted: 7 March 2023

Published: 10 March 2023



Copyright: © 2023 by the authors. Licensee MDPI, Basel, Switzerland. This article is an open access article distributed under the terms and conditions of the Creative Commons Attribution (CC BY) license (<https://creativecommons.org/licenses/by/4.0/>).

1. Introduction

Tetrazoles are organic compounds that contain a five-membered ring of four nitrogen atoms and one carbon [1–3]. They exist in two tautomeric forms: the 1*H*- form is the more stable and abundant in solution; the equilibrium shifts toward the 2*H*- form in the gas phase [1,3]. Tetrazoles have garnered interest over the years due to their compelling properties, namely their rich nitrogen content, low basicity, high acidity, high stability, and formation enthalpy [4]. These properties make tetrazoles suitable candidates as ligands for metal ions due to their expansive coordination ability [5], as surrogates for carboxylic acids in drug design [6], due to similar p*K_a* figures and greater lipophilicity, and as high energy materials [7]. Their scope of application broadens to include both homogeneous catalysis, where tetrazoles coordinate to metal centers to form metallo-organic complexes [8–10], and heterogeneous catalysis, where those complexes are attached to a solid support [11–13].

Among 5-R-tetrazole derivatives, 5-(pyridyl)tetrazoles have attracted attention as ligands owing to their multiple coordination modes, which expand the coordination chemistry of the tetrazole fragment. In the case of 5-(2-pyridyl)tetrazole (Hptz), the pK_a of the pyridyl N atom ($pK_a = 5.25$) is very similar to that of N1 of the tetrazolyl ring ($pK_a = 4.9$), which increases the proclivity of the molecule to coordinate as a bidentate ligand to metal centers [14]. This coordination mode is the most common among nine different possibilities [15], enabled by the deprotonation of Hptz to the tetrazolate anion (ptz^-). In practical terms, this can lead to numerous chelating and bridging coordination modes [15–17] to give molecular complexes, multinuclear clusters, and extended one-dimensional (1D), 2D, and 3D structures with various d-block metals [18].

We previously prepared the complex salt $(H_2ptz)[MoO_2Cl_2(ptz)]$ and the microcrystalline molybdenum oxide/organic hybrid $[MoO_3(Hptz)]$, which were assessed for their potential as catalysts of the epoxidation of biomass-derived olefins [19]. In the epoxidation of the model olefin *cis*-cyclooctene, the former acted as a homogeneous catalyst, and the latter as a heterogeneous one. With a *cis*-cyclooctene oxide yield of 100%, $[MoO_3(Hptz)]$ was further tested for the conversion of the monoterpene *dl*-limonene (LIM) and the biobased unsaturated fatty acid methyl esters (FAMES) methyl oleate (MO) and methyl linoleate (ML), which mostly resulted in epoxide products. In addition, we integrated Hptz in the preparation of a polyoxometalate-based hybrid, namely a silicododecamolybdate/pyridinium-tetrazole hybrid molecular salt, where Hptz acted as the starting reagent that produced the counteranion 2-(tetrazol-5-yl)pyridinium [20]. The salt behaved as a homogeneous catalyst in the epoxidation of *cis*-cyclooctene, leading to a quantitative yield of *cis*-cyclooctene oxide. It likewise proved to be an effective catalyst for the conversion of biomass-derived olefins, specifically LIM, MO, and ML, into epoxides, diepoxides, and diol products, which are high-added-value compounds in the production of specialty and commodity chemicals [21–23] as well as pharmaceuticals [24,25].

The oxidation of Hptz enables the further exploration of the chemistry associated with Hptz in a targeted manner. Facchetti et al. successfully prepared 5-(2-pyridyl-1-oxide)tetrazole (Hpto) by mixing Hptz with 3-chloroperoxybenzoic acid in methanol [26]. This oxidant selectively targets the pyridyl N atom, unlike others such as H_2O_2 and CH_3CO_3H , which form inseparable mixtures of products. The interaction between Hpto and bases originates the anion 5-(2-pyridyl-1-oxide)tetrazolate (pto^-) [26–29]. To the best of our knowledge, the metallo-organic complexes reported in the literature involve the ligand Hpto as an anion, with lanthanide ions Eu(III) [27,28], Gd(III) [26–28], and Tb(III) [27] for luminescence purposes, and transition metal ions Zn(II) [26] and Mn(II) [29]. These structures share common bidentate coordination of pto^- to the metal center, specifically N(py)-O-M and N1(tz)-M (py = pyridyl ring, tz = tetrazolate ring).

As a related compound of Hptz, it is worthwhile to investigate the performance of Hpto as a ligand in inorganic/organic catalysts for olefin epoxidation, a field where Hptz has yielded encouraging results. In this work, we report the synthesis of the new compounds $[MoO_2Cl_2(Hpto)] \cdot THF$ (**1**) and $[MoO_3(Hpto)] \cdot H_2O$ (**2**). To the best of our knowledge, these are the first inorganic/organic compounds where Hpto coordinates in its neutral form to a group 6 transition metal, i.e., molybdenum.

2. Results and Discussion

2.1. Synthesis and Characterization

The structure of the ligand Hpto was determined by single-crystal X-ray diffraction (XRD), with the compound crystallizing in the centrosymmetric space group $P2_1/n$. The asymmetric unit is composed of two independent Hpto molecules, both having the tetrazole ring in its neutral form (Figure 1). The hydrogen atom of one of the tetrazole rings is disordered, appearing at both N2 and N5 with a 70% and 30% occupancy rate, respectively. The crystal packing is mediated mainly by weak intermolecular hydrogen-bonding interactions (all of the C–H...N kind—see Table S1 for more information) and strong π - π interactions [$d_{\pi \dots \pi} = 3.646(3)$ Å]. These latter interactions arise between a pair of pyridyl

rings and a pair of tetrazole rings, assisted by the almost planar configuration of the Hpto molecules (the dihedral angle between the planes formed by the aromatic and tetrazole rings is $3.612(3)^\circ$), resulting from the strong intramolecular N–O \cdots H interactions (Figure 1).

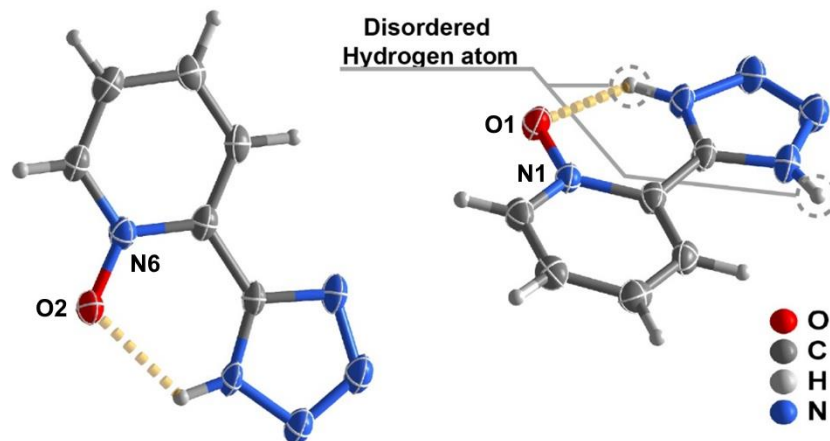


Figure 1. Schematic representation, with selected atomic labelling, of the asymmetric unit of Hpto, emphasizing the disordered hydrogen atom in one of the tetrazole rings. All non-hydrogen atoms are represented as displacement ellipsoids drawn at the 50% probability level and hydrogen atoms as small spheres with arbitrary radii. N–O \cdots H intramolecular interactions are represented by dashed orange lines. Selected bond distances (Å): N1–O1 1.307(5); N6–O2 1.302(5).

The treatment of a solution of the solvent adduct $[\text{MoO}_2\text{Cl}_2(\text{THF})_2]$ (prepared by dissolving MoO_2Cl_2 in THF) with one equivalent of Hpto gave the compound $[\text{MoO}_2\text{Cl}_2(\text{Hpto})]\cdot\text{THF}$ (**1**). Single crystals of **1** suitable for XRD were obtained by the slow diffusion of diethyl ether into a solution of the complex in THF. The compound crystallized in the centrosymmetric space group $P2_1/c$, with the asymmetric unit being composed of the molybdenum complex and one tetrahydrofuran molecule of crystallization (Figure 2). The Mo atom is hexacoordinated by a Hpto molecule, two oxo groups, and two chloride anions, with a $\{\text{MoO}_3\text{NCl}_2\}$ coordination sphere resembling a distorted octahedron. The Hpto molecule is, in turn, coordinated to the metal center in a bidentate fashion by way of a *N,O*-chelate. This coordination mode is responsible for the non-planar nature of the Hpto ligand, showing a rotation between the pyridyl and tetrazole rings with a dihedral angle of 16.85° . The N–O distance of $1.334(2)$ Å in the complex is slightly longer than that in the free ligand ($1.302(5)$ Å, $1.307(5)$ Å). Complexes with (H)pto are rare, with only Gd^{III} , Zn^{II} , and Mn^{II} structures [26,29] being reported to date according to a search in the Cambridge Structural Database [30]. While the two M^{II} complexes have an octahedral coordination sphere, they are diaqua complexes with two coordinated pto $^-$ molecules. The presence of two *N,O*-chelated moieties in these complexes leads to a less distorted octahedron when compared with that of compound **1**.

To the best of our knowledge, only one other literature structure exists for complexes of the type $[\text{MoO}_2\text{Cl}_2(\text{L})_n]$ containing a pyridine *N*-oxide ligand, namely $[\text{MoO}_2\text{Cl}_2(4\text{-MepyO})_2]$ (4-MepyO = 4-methylpyridine-1-oxide) [31]. The Mo–O(pyO) bond lengths found for this complex (2.166 Å, 2.189 Å) are similar to those determined for **1** (2.155 Å).

The close packing of the individual moieties composing **1** is mostly mediated by weak supramolecular interactions (C–H \cdots Cl and C–H \cdots O; see Table S2 for more information), with the complex units forming hexagonal “channels” parallel to the *a*-axis of the unit cell, filled with the THF crystallization solvent molecules (Figure 3). These molecules maintain, however, strong connections with the complexes by way of hydrogen bonding between the oxygen atom in the THF molecule and the hydrogen atom of the tetrazole ring [$d_{\text{N-H}\cdots\text{O}} = 2.619(2)$ Å].

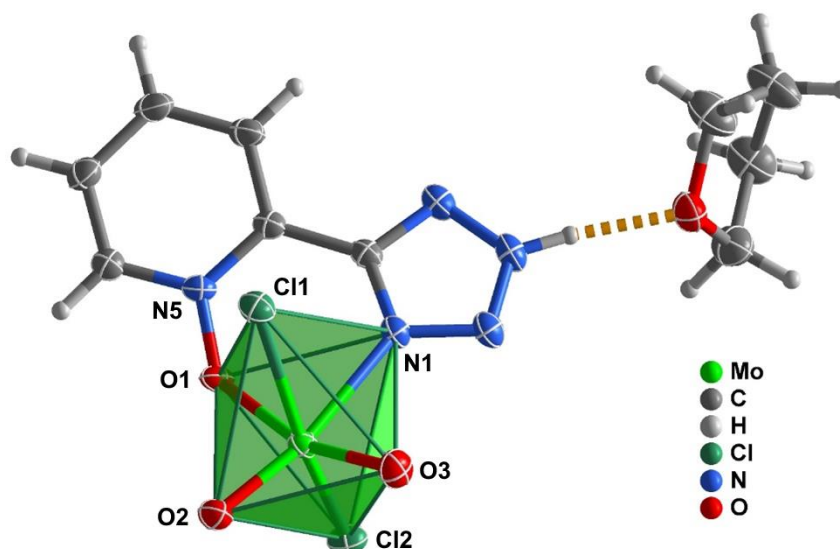


Figure 2. Schematic representation, with selected atomic labelling, of the asymmetric unit of compound $[\text{MoO}_2\text{Cl}_2(\text{Hpto})]\cdot\text{THF}$ (**1**), showing all non-hydrogen atoms as displacement ellipsoids drawn at the 70% probability level and hydrogen atoms as small spheres with arbitrary radii. The hydrogen bonding interaction between the molybdenum complex and the THF molecule is depicted as a dashed orange line. Selected bond distances (\AA): Mo1-Cl1 2.4012(6); Mo1-Cl2 2.3623(6); Mo1-N1 2.339(1); Mo1-O1 2.155(1); Mo1-O2 1.704(1); Mo1-O3 1.689(2); N5-O1 1.334(2). Selected bond angles ($^\circ$): O3-Mo1-O2 104.53(7); O3-Mo1-O1 160.38(6); O2-Mo1-O1 95.04(6); O2-Mo1-N1 167.60(6); O3-Mo1-N1 87.62(6); Cl1-Mo1-Cl2 159.811(17); O1-Mo1-N1 72.77(5); Mo1-O1-N5 130.93(10).

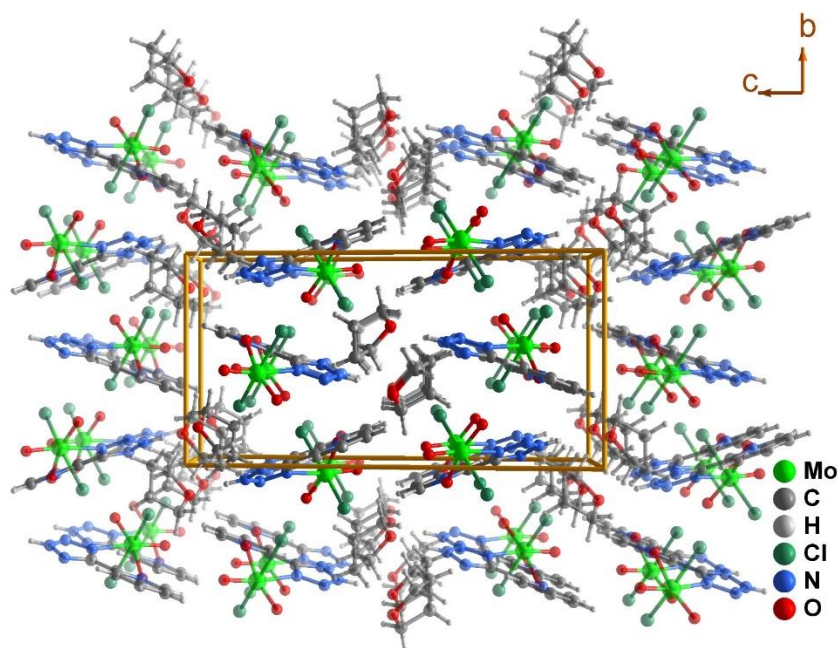


Figure 3. Schematic representation of the crystal packing of compound $[\text{MoO}_2\text{Cl}_2(\text{Hpto})]\cdot\text{THF}$ (**1**) viewed in perspective along the $[100]$ direction of the unit cell.

The FT-IR spectrum of **1** displays a strong band at 909 cm^{-1} , assigned to $\nu_{\text{asym}}(\text{Mo}=\text{O})$, and a weaker one at 944 cm^{-1} , assigned to $\nu_{\text{sym}}(\text{Mo}=\text{O})$, confirming the presence of a $\text{cis-}[\text{MoO}_2]^{2+}$ unit (Figure 4A). The corresponding bands appear in the Raman spectrum at 913 and 946 cm^{-1} with weak and strong intensity, respectively (Figure 4B). For comparison, the complex $(\text{H}_2\text{ptz})[\text{MoO}_2\text{Cl}_2(\text{ptz})]$ displayed a similar pair of bands at $914\text{--}915\text{ cm}^{-1}$ and

$945 \pm 1 \text{ cm}^{-1}$ [19]. These frequencies are typical for complexes of the type $[\text{MoO}_2\text{Cl}_2(\text{L})]$ containing bidentate Lewis-base ligands.

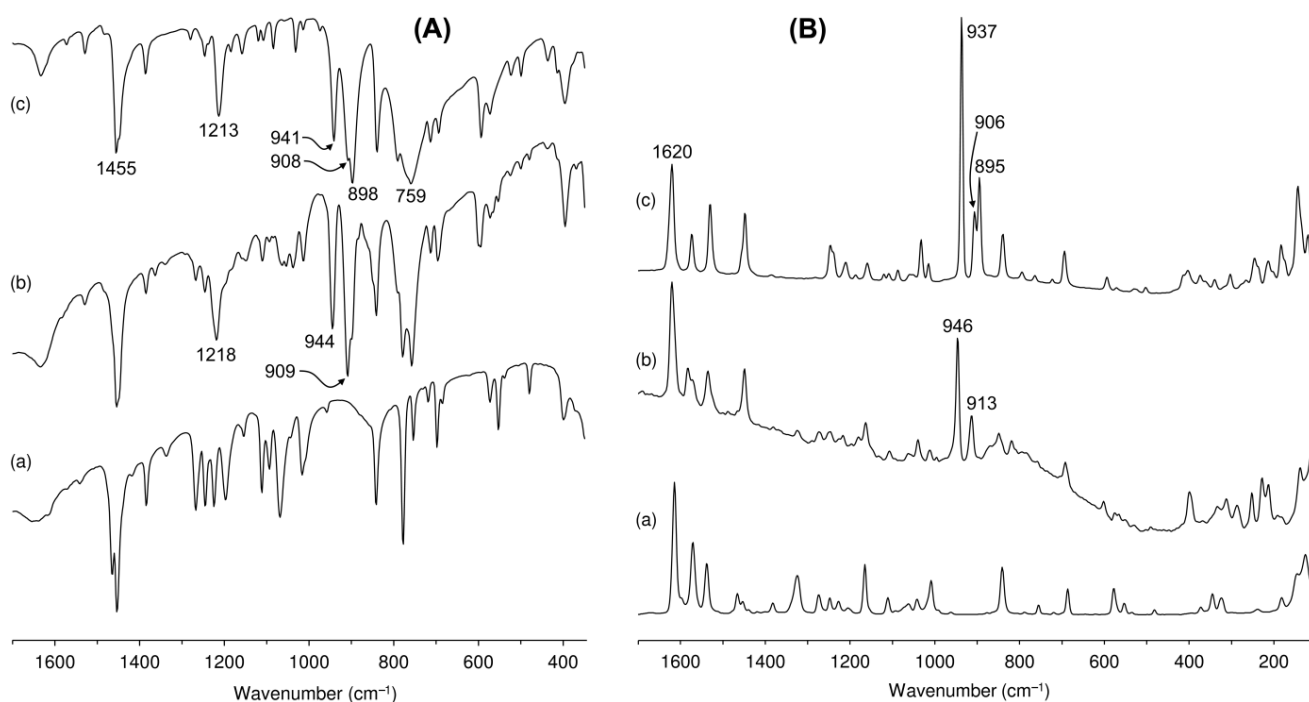


Figure 4. FT-IR spectra in the range of $350\text{--}1700 \text{ cm}^{-1}$ (A) and Raman spectra in the range of $100\text{--}1700 \text{ cm}^{-1}$ (B) of (a) ligand Hpto, (b) complex **1**, and (c) compound **2**.

A $^1\text{H}\text{--}^{13}\text{C}$ HSQC NMR experiment was performed for the free ligand Hpto to allow for the unambiguous assignment of the respective 1D spectra (Figure S1). The solid-state $^{13}\text{C}\{^1\text{H}\}$ CP MAS NMR spectrum of Hpto was interpreted in accordance with the assignments made for the solution spectrum, with three distinct peaks being observed for the tetrazole carbon atom (Ctz) and the pyridyl carbon atoms directly bond to nitrogen (C2 and C6), while the resonances for the remaining three pyridyl carbons (C3, C4, and C5) overlapped to give one intense peak centered at 127.9 ppm, with a shoulder at 127.0 ppm (Figure 5). The solid-state $^{13}\text{C}\{^1\text{H}\}$ CP MAS NMR spectrum of complex **1** is consistent with the bidentate coordination of Hpto to the Mo^{VI} center since the resonance for Ctz is shifted strongly downfield by 6.3 ppm relative to that for the free ligand. The remaining pyridyl carbon signals are tentatively assigned on the basis that the resonances for C3, C5, and C6 undergo minor downfield shifts of less than 1.3 ppm relative to those for Hpto, while the resonances for C2 and C4 are downfield-shifted by about 4 and 9 ppm, respectively. Two sharp resonances are observed at 26.5 and 69.4 ppm for the THF molecules of crystallization.

In previous work, we have explored the hydrolysis–condensation–polymerization chemistry of dichloro complexes of the type $[\text{MoO}_2\text{Cl}_2(\text{L})]$ containing N-heterocyclic aromatic ligands (L) [19,32–37]. The treatment of these complexes with water led to the synthesis of molybdenum oxide/organic hybrid materials with the formulas $\{[\text{MoO}_3(\text{bipy})][\text{MoO}_3(\text{H}_2\text{O})]\}_n$ (bipy = 2,2'-bipyridine) [32], $[\text{Mo}_8\text{O}_{22}(\text{OH})_4(4,4'\text{-di-tert-butyl-2,2'-bipyridine})_4]$ [33], $[\text{Mo}_2\text{O}_6(3\text{-pyridinium-2-yl-1H-pyrazol-1-yl}]\text{acetate})]$ [34], $[\text{Mo}_3\text{O}_9(2\text{-[3(5-pyrazolyl)]pyridine})]_n$ [35], $[\text{Mo}_2\text{O}_6(2\text{-[1-pentyl-3-pyrazolyl]pyridine})]$ [36], $[\text{MoO}_3(2\text{-[2-pyridyl-benzimidazole})]$ [37], and $[\text{MoO}_3(\text{Hptz})]$ [19]. In a similar fashion, compound **1** was treated with water under reflux for 16 h, affording an insoluble white solid (**2**) suspended in an acidic mother liquor (pH = 1–2). The low pH of the solution is due to the presence of HCl resulting from the hydrolysis of the Mo–Cl bonds in **1**. The white color suggests that the oxidation state of molybdenum in catalyst **2** is 6+.

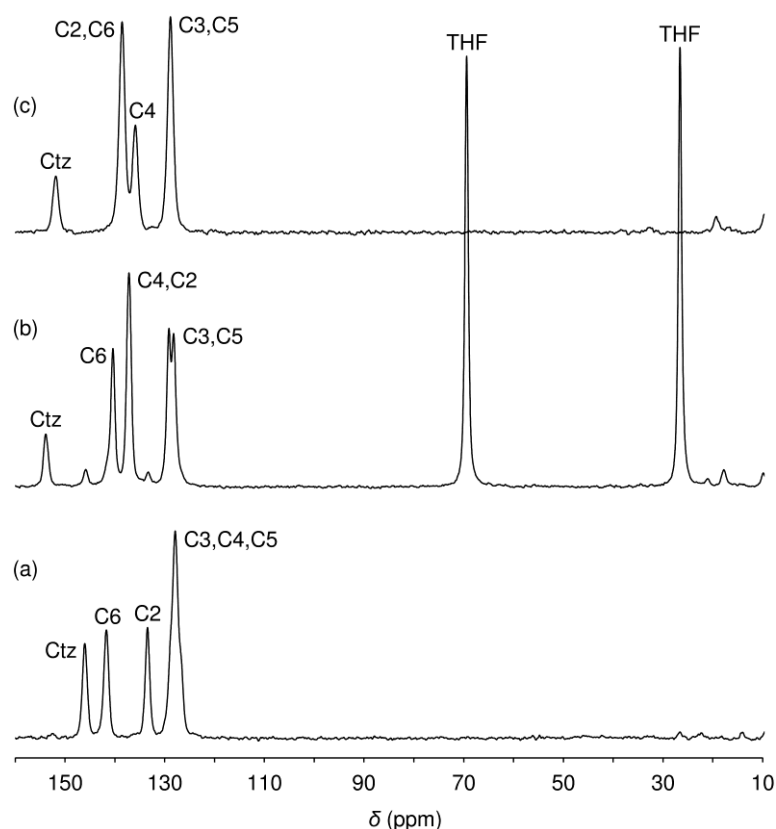


Figure 5. $^{13}\text{C}\{^1\text{H}\}$ CP MAS NMR spectra of (a) ligand Hpto, (b) complex **1**, and (c) compound **2**.

Powder XRD showed that material **2** was microcrystalline but with a different crystal structure from that of the precursor **1** (Figure 6B). The solubility of the precursor **1** in water is too low and the hydrolysis process too fast to allow for the growth of single crystals of **2** suitable for X-ray diffraction, i.e., compound **2** readily precipitates as a fine microcrystalline solid upon formation. Microanalyses (C,H,N) and Mo content determination by ICP-OES indicated the formula $[\text{MoO}_3(\text{Hpto})]\cdot\text{H}_2\text{O}$. SEM-EDS analyses and elemental mapping confirmed the absence of chlorine in **2**. Hybrid **2** possessed a specific surface area of $73\text{ m}^2\text{ g}^{-1}$, pore volume of $0.117\text{ cm}^3\text{ g}^{-1}$, and did not possess measurable microporosity. The N_2 sorption isotherm indicated increasing N_2 uptake in the full range of relative pressure (p/p_0) and a steep uptake as p/p_0 approached unity, suggesting that the material is non-porous and/or possesses very large mesopores (2–50 nm) or macropores (>50 nm) (Figure S2a). The pore size distribution curve showed several peaks in the range of 2–17 nm and some broad weak peaks in the macropore size range (Figure S2b), which may be associated with open interparticle void spaces.

At the present time, the structure of **2** has not been completely resolved. However, the presence of a molybdenum oxide substructure in the compound is indicated by the $720\text{--}1000\text{ cm}^{-1}$ region of the FT-IR and Raman spectra, which contain several bands assigned to $\nu(\text{Mo}=\text{O})$ ($895\text{--}898$, $906\text{--}908$ and $937\text{--}941\text{ cm}^{-1}$) and, in the case of the IR spectrum, a broad band centered at 759 cm^{-1} that is attributed to a $\nu(\text{Mo}\text{--}\text{O}\text{--}\text{Mo})$ vibrational mode, confirming that **2** possesses a condensed (polymeric) structure (Figure 4). Concerning the spectral region containing the ligand modes, i.e., $1000\text{--}1700\text{ cm}^{-1}$, the similarity between the spectra of **1** and **2** suggests that the *N,O*-chelating mode of the ligand in **1** is maintained in **2**, i.e., bidentate coordination of the ligand to a Mo^{VI} center. Both **1** and **2** display a Raman band at 1620 cm^{-1} and an IR band at 1455 cm^{-1} , assigned to the $\nu(\text{C}=\text{C})$ and $\nu(\text{N}=\text{C})/\nu(\text{N}=\text{N})$ stretching vibrations of the tetrazole ring, respectively. The medium-intensity IR bands at 1218 cm^{-1} for **1** and 1213 cm^{-1} for **2** are assigned to N-O stretching vibrations. The confirmation of the presence of similar Hpto coordination modes in **1** and **2** is provided by the solid-state $^{13}\text{C}\{^1\text{H}\}$ CP MAS NMR spectra, which show differences

of only 2 ppm or less in the chemical shifts for the tetrazole and pyridyl carbon atoms (Figure 5).

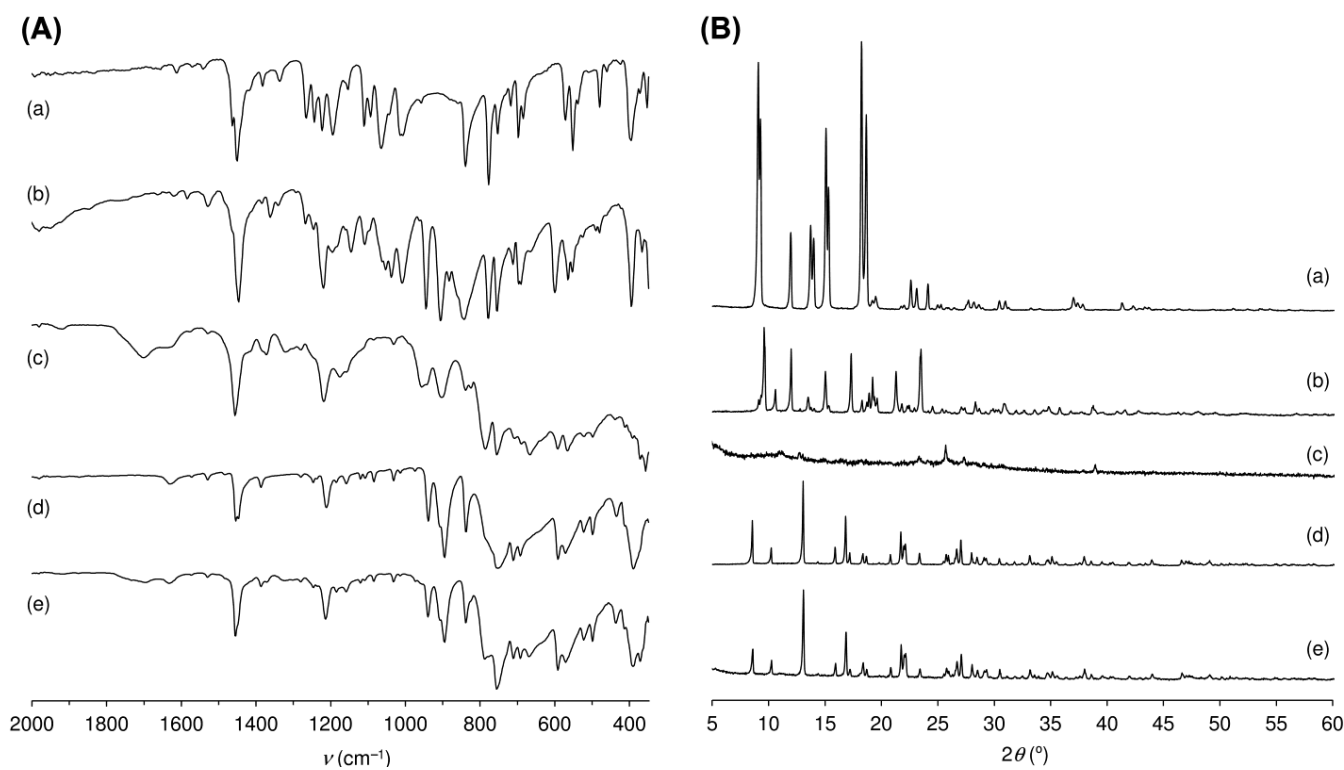


Figure 6. ATR FT-IR spectra (A) and powder XRD patterns (B) of (a) Hpto, (b) **1**, (c) **1**-used, (d) **2**, and (e) **2**-used.

2.2. Catalytic Studies

2.2.1. Epoxidation of *cis*-Cyclooctene

The catalytic properties of complex **1** and the hybrid **2** were firstly studied using the model epoxidation reaction of *cis*-cyclooctene (Cy8) at different temperatures (55 and 70 °C). *tert*-Butyl hydroperoxide (TBHP) and α,α,α -trifluorotoluene (TFT) were chosen as oxidant and solvent, respectively, due to their favorable properties in epoxidation systems. TBHP may be produced from renewable sources, has a growing market with commercial applications such as the large-scale epoxidation of propene [38,39], and presents as main advantages its compatibility with organic media, stability, and the fact that the co-product is *tert*-butanol, which can be repurposed. Moreover, as discussed below, catalytic stability may be higher when using TBHP, whereas H₂O₂ may promote the decomposition and solubilization of the molybdenum compounds [37,40–42]. On the other hand, the hydrophobicity, relatively high boiling point (102 °C), and insignificant coordinating properties of TFT make it more appealing than volatile halogenated solvents, which contribute to atmospheric emissions (with damaging environmental impacts), or coordinating solvents, which may compete with the reactants for access to the active sites [43].

Compounds **1** and **2** led to cyclooctene oxide (Cy8O) as the only product (100% Cy8O selectivity, Figure 7A). Without a catalyst and/or without TBHP, the reactions were negligible. For each compound, increasing the reaction temperature from 55 to 70 °C led to a much faster epoxidation reaction. On the other hand, for each reaction temperature, the catalytic reaction was much faster in the presence of **1**, giving, at 70 °C, a quantitative yield of Cy8O within 1 h, whereas **2** led to a 90% Cy8O yield at 6 h.

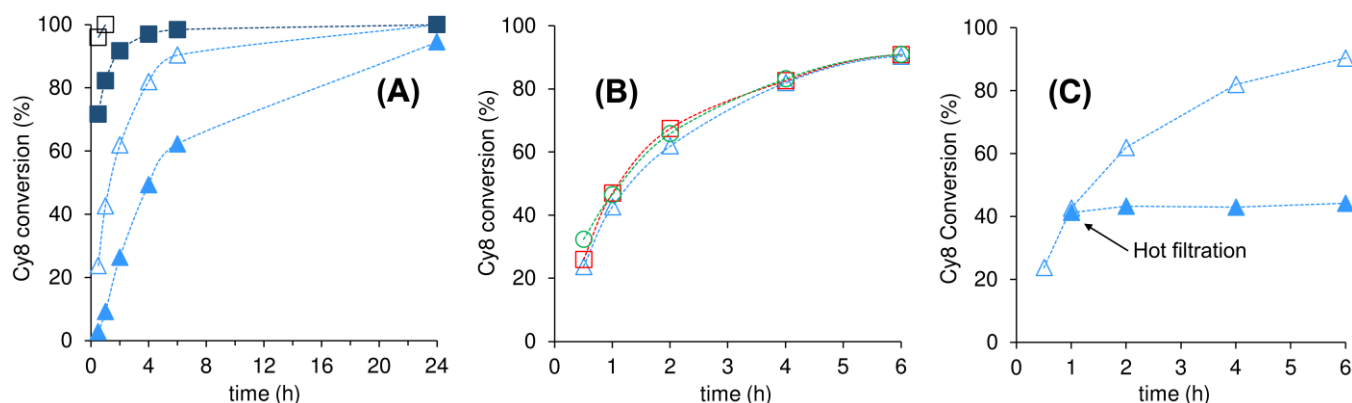


Figure 7. *Cis*-cyclooctene (Cy8) epoxidation with TBHP in TFT for the systems: (A) 1/55 °C (■), 1/70 °C (□), 2/55 °C (▲), and 2/70 °C (△); (B) 2/70 °C (run 1 (△), run 2 (□), run 3 (○)); (C) 2/70 °C (normal run (△) and leaching test (▲)). Dashed lines are visual guides. Cy8O was the only product formed for all reactions (Cy8O selectivity = 100%).

A leaching test for **1** (at 55 °C) confirmed that it was a homogeneous catalyst; specifically, the increment in Cy8 conversion between 0.5 h and 6 h was 20%, which is similar to that without catalyst filtration, i.e., a normal catalytic batch run (27%).

The catalytic results for **1** are comparable with those reported for the ionic complex $(\text{H}_2\text{ptz})[\text{MoO}_2\text{Cl}_2(\text{ptz})]$ (100% epoxide yield at 1 h) [19]. Both complexes led to homogeneously catalyzed reactions. The reaction with **1**, at 70 °C, led to the formation of an insoluble and largely amorphous solid (designated as **1-used**) with a powder XRD pattern containing only a few very weak reflections (different from those displayed by microcrystalline **1**; Figure 6B). Structural changes are also indicated by the different ATR FT-IR spectra of **1** and **1-used** (Figure 6A).

In contrast to the results with **1**, the hybrid material **2** exhibited high chemical and structural stability, i.e., the ATR FT-IR spectrum and powder XRD pattern of the solid recovered after the catalytic run of 24 h (**2-used**) were practically unchanged from those of the as-prepared **2** (Figure 6). Two further consecutive batch runs, at 70 °C, were performed (starting with **2-used**) and the kinetic curves for all three runs were roughly coincident (Figure 7B). Based on SEM, the particle sizes of **2** seemed to decrease during the catalytic process (Figure 8), although this did not affect the reaction kinetics, which somewhat suggests that the overall reaction system advantageously operates under a kinetic regime. A leaching test for **2** indicated no significant increment in conversion after separating the solid catalyst from the reaction mixture after 1 h, at the reaction temperature, suggesting that **2** performs essentially as a stable solid catalyst (Figure 7C). Based on the characterization studies, **2** does not possess measurable microporosity, but possesses meso-macropores that may correspond to interparticle void spaces, suggesting that the catalytic reaction likely occurs on the external surface.

Very few of the $[\text{MoO}_3\text{L}]$ -type hybrids described in the literature exhibited heterogeneous catalytic features [19,44,45]. The results for **2** (82%/100% epoxide yield at 4 h/24 h) are comparable with those reported for the hybrid heterogeneous catalyst $[\text{MoO}_3(\text{Hptz})]$ (89%/100% epoxide yield at 5 h/24 h) [19].

Changing the oxidant from TBHP to H_2O_2 at 70 °C led not only to a much slower Cy8 reaction (conversion at 24 h was of 60% for **1**, and 81% for **2**) but also to homogeneous catalytic systems, i.e., yellow solutions were obtained for the systems **1**/ H_2O_2 and **2**/ H_2O_2 , indicating that **1** and **2**, respectively, are unstable in the presence of H_2O_2 . Based on the conversion at 24 h/70 °C, the catalytic results for **2**/ H_2O_2 are in the mid-range of what is typically found for $[\text{MoO}_3(\text{L})_x]$ -type polymeric hybrids tested for Cy8/ H_2O_2 epoxidation [37,40,41,46,47]. The hybrids reported in the literature acted as homogeneous catalysts with the exception of three materials which acted as reaction-induced self-separating catalysts, namely $[\text{MoO}_3(\text{tradCH})\cdot\text{H}_2\text{O}]$ (tradCH = 1,2,4-triazol-4-yl)adamantane-1-carboxylic

acid) [48], $[\text{MoO}_3(\text{trleuH})] \cdot 0.5\text{H}_2\text{O}$ (trleuH = *dl*-4-methyl-2-(4H-1,2,4-triazol-4-yl)pentanoic acid) [49], and $[\text{MoO}_3(1,2,4\text{-trz})_{0.5}]$ (1,2,4-trz = 1,2,4-triazole) [50].

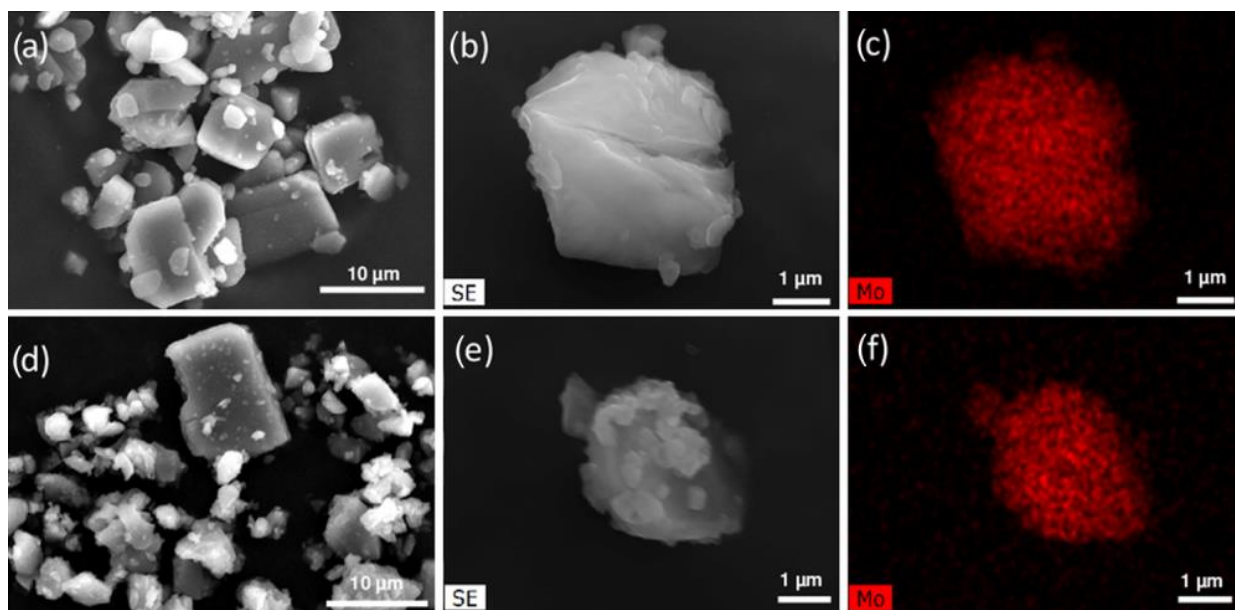


Figure 8. SEM images (a,b,d,e) and molybdenum maps (c,f) of **2** (a–c) and **2**-used (d–f) (Cy8/TBHP/TFT/70 °C).

For the system Cy8/TBHP/**2**, changing the solvent from TFT to ethyl acetate (a renewable solvent owing to, for example, bioethanol-based production processes [51]) led to slower reaction kinetics (90% and 67% conversion, respectively, at 6 h). Hence, further catalytic studies were carried out with TBHP/TFT.

2.2.2. Epoxidation of Biobased Olefins

Catalyst **2** was further explored for the challenging practical goal of the chemical valorization of renewable vegetable oils (VOs) and *dl*-limonene (LIM) via mild, selective catalytic routes. FAMES are formed via (trans)esterification of VOs which may be obtained from the edible parts of agricultural crops (e.g., soybean oil), non-edible raw materials such as waste from the forest industry and waste cooking oil, and oil-producing microalgae [52]. The terpene LIM is one of the main components of citrus peel waste (up to 4% by weight) and it is estimated that every year 110–120 million tons of citrus waste is generated worldwide from citrus-processing industries [53].

The epoxidation of FAMES and LIM with TBHP, in the presence of **2**, was studied at 70 °C. The FAME substrate scope included the monoene methyl oleate (MO), the diene methyl linoleate (ML), the triene methyl linolenate (MLN), and the hydroxy-FAME methyl ricinoleate (MR). Catalyst **2** was very active for the epoxidation of the biobased olefins (Table 1, Figure 9). LIM was converted to LIMox which was formed in 100%/72% selectivity at 38%/100% conversion, reached at 30 min/6 h (Figure 9A,B, Table 1). As LIM conversion increased, LIMox was converted to LIMdiox and limonene diol (LIMdiol) (25% and 3% selectivity, respectively, at 100% conversion, 6 h). Hence, the epoxidation of the more electron-rich endocyclic double bond (position 1,2) was more favorable than that of the exocyclic double bond (position 8,9). This regioselectivity is consistent with mechanistic studies reported in the literature for olefin epoxidation using hydroperoxide oxidants (ROOH) in the presence of organo-oxomolybdenum catalysts. An associative mechanism may occur where the metal center acts as a Lewis acid for ROOH activation, forming an active oxidizing species that is responsible for an electrophilic oxygen atom transfer step to the olefin substrate, leading to the formation of the epoxide product [54]. In this process,

more electron-donating groups increase the electron density at the C=C bond of the olefin, making it more susceptible to epoxidation.

Table 1. Catalytic results for olefin epoxidation at 70 °C and sulfide oxidation at 35 °C, in the presence of **2** using TBHP as oxidant.

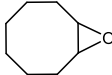
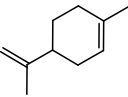
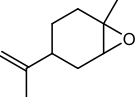
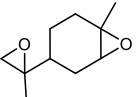
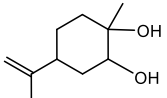
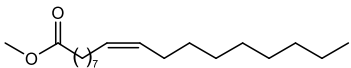
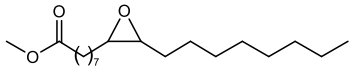
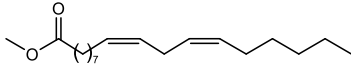
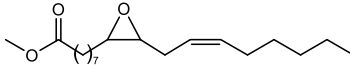
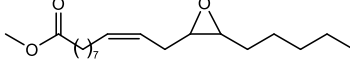
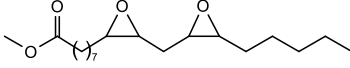
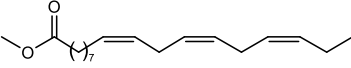
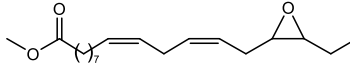
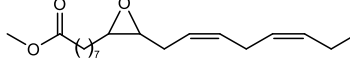
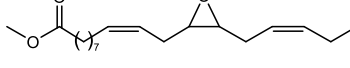
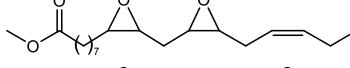
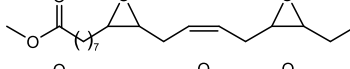
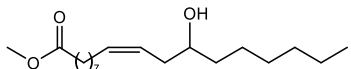
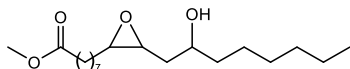
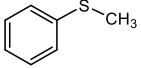
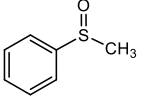
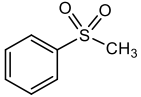
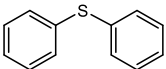
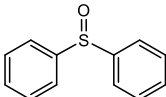
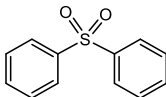
	Substrate ^a	Conversion (%)		Product(s)	Selectivity (%)	
		6 h	24 h		6 h	24 h
Cy8		90	100		100	100
<i>dl</i> -LIM		100	100		72	59
					25	33
					3	8
MO		90	96		100	100
ML		68	88		85	65
						
					15	32
MLN		79	94		69	44
						
						
					31	50
						
Others					0	6
MR		92	100		100	100

Table 1. Cont.

	Substrate ^a	Conversion (%)		Product(s)	Selectivity (%)	
		6 h	24 h		6 h	24 h
MPS		100	100		77	14
					23	86
DPS		100	100		67	23
					33	77

^a Initial Mo:substrate:TBHP molar ratio = 1:100:153 (for Cy8) or 1:100:210 (remaining substrates), 1 mL TFT.

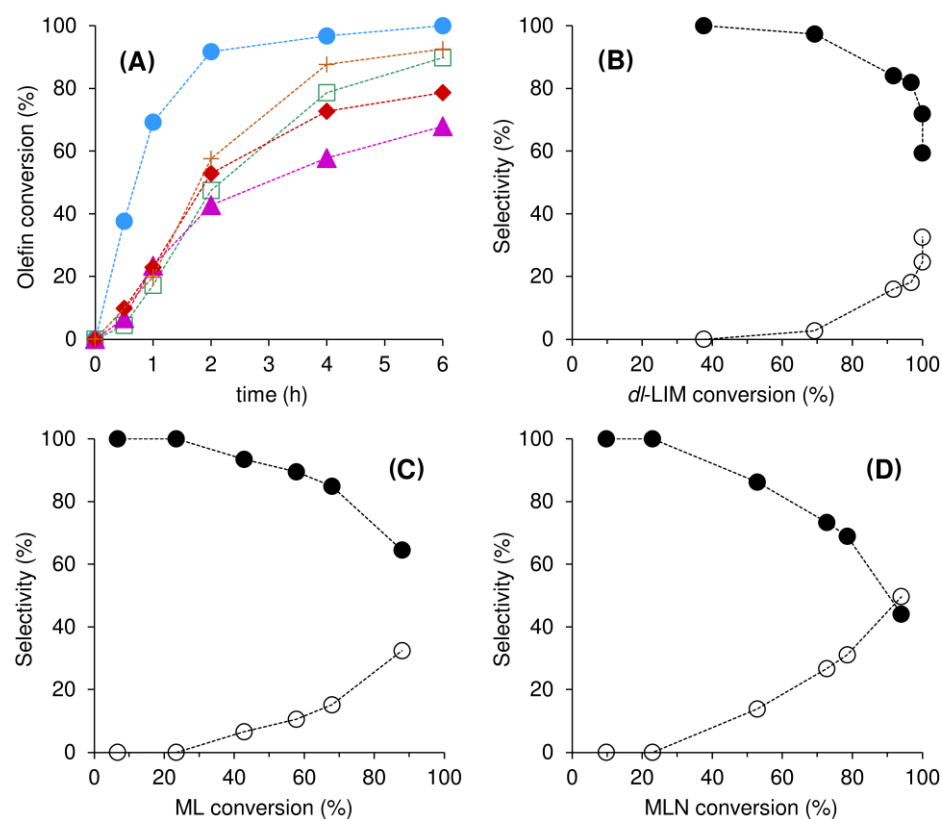


Figure 9. Kinetic profiles for the reaction of *dl*-limonene (●), methyl oleate (□), methyl linoleate (▲), methyl linolenate (◆), and methyl ricinoleate (+) with TBHP, in the presence of **2**, at 70 °C (A), and selectivity to the monoepoxides (●) and diepoxides (○) of LIM (B), ML (C), and MLN (D) as a function of olefin conversion. Dashed lines are visual guides.

With MO as substrate, **2** led to 100% selectivity of the corresponding monoepoxide, methyl 9,10-epoxyoctadecanoate (MOox), at 96% conversion, 24 h (Table 1, Figure 9). More complex product mixtures were obtained with the polyfunctional FAMES ML and MLN. With MLN, the selectivity to total monoepoxides (MLN_{ox} = methyl 15,16-epoxy-9,12-octadecadienoate + methyl 12,13-epoxy-9,15-octadecadienoate + methyl 9,10-epoxy-

12,15-octadecadienoate) decreased from 100% at 23% conversion (reached at 1 h) to 44% at 94% conversion (24 h), which was accompanied by the formation of diepoxides MLNdiox (50% selectivity), where MLNdiox = methyl 9,10-15,16-diepoxy-12-octadecenoate + methyl 12,13-15,16-diepoxy-9-octadecenoate + methyl 9,10-12,13-diepoxy-15-octadecenoate, and other unidentified products (total selectivity of 6%, which possibly includes the triepoxide methyl 9,10-12,13-15,16-triepoxyoctadecanoate) (Table 1, Figure 9A,D).

For catalyst 2 with ML as substrate, the selectivity to the corresponding monoepoxides (MLox = methyl 12,13-epoxy-9-octadecenoate and methyl 9,10-epoxy-12-octadecenoate) decreased from 100% at 7% conversion (1 h) to 65% at 88% conversion (24 h), with the concomitant formation of diepoxides (MLdiox = methyl 9,10,12,13-diepoxy-octadecanoate) with 32% selectivity at 88% conversion (Table 1, Figure 9A,C); minor products (3% total selectivity) included cyclization hydroxytetrahydrofuranic compounds (MLcycl = methyl 10,13-epoxy-9,12-dihydroxy-octadecanoate + methyl 9,12-epoxy-10,13-dihydroxy-octadecanoate).

For each substrate, ML and MLN, the respective monoepoxide isomers (at positions 9,10 or 12,13 for ML, and 9,10 or 12,13 or 15,16 for MLN) were formed in equimolar amounts, suggesting that the C=C bonds for each substrate possessed similar nucleophilicity.

The reaction of methyl ricinoleate (MR) gave solely the corresponding epoxide (MRox = methyl-9,10-oxido-12-hydroxyoctadecanoate), formed in 92%/100% yield at 6 h/24 h, 70 °C (Table 1, Figure 9A). These results are similar to those with MO as substrate. Similar reactivities of MR and MO were previously reported for a system using MoO₃/alumina with TBHP [55], while somewhat different reactivities (MR > MO) were reported for a system using Mo(CO)₆ with cumyl hydroperoxide as oxidant [56]. Overall, 2 was effective for the epoxidation of unsaturated FAMES, which occurred to different extents. Conversion at 6 h/70 °C decreased in the following order: MO (90%) > MLN (79%) > ML (68%); after 24 h, the conversions of MO and MLN were still higher (94–96%) than that of ML (88%; Table 1, Figure 9). Studies in the literature reported different orders of reactivities of the three FAMES [57–61]. Those with a greater number of C=C bonds per molecule exhibited higher reactivity for systems using formic acid, acetic acid+H₂SO₄ [57], or Nb-silica catalysts [58], with H₂O₂ as oxidant. The trend MO > ML > MLN was reported for oxovanadium complexes with TBHP [59], or formic acid with H₂O₂ [60]. For a Venturello catalyst using H₂O₂, no clear trend could be established [61]. Electron-donating groups adjacent to C=C bonds may increase the FAME reactivity. On the other hand, for polyfunctional olefins, a greater number of C=C bonds may facilitate consecutive epoxidation reactions (especially using catalysts with a high density of active sites), which may negatively impact the substrate reaction rate.

In parallel with that verified with Cy8 as substrate, the precursor to 2, i.e., complex 1, was more active than 2 for the epoxidation of the biobased olefins (MO, LIM), although, as discussed above, the former performed as a homogeneous catalyst. In the presence of 1, LIM was completely converted at 2 h, giving mainly mono and diepoxides in 84% total yield (LIMox/LIMdiox = 4), whereas 2 led to 92% conversion at 2 h (mono and diepoxides in 100% total yield). While 1 led to 97% MOox yield at 4 h, the hybrid 2 led to 79% MOox yield (100% selectivity for MOox using both catalysts).

Table 2 compares the catalytic results for 2 to literature data for the epoxidation of the biobased olefins, in the presence of homogeneous and heterogeneous [MoO₃(L)_x]-type catalysts [19,37,44,62,63]. To the best of our knowledge, 2 is the first [MoO₃(L)_x]-type catalyst to be studied for the reactions of MLN and MR. The results for the reaction of MO in the presence of 2 (using TFT at 70 °C) are superior or comparable to literature data (entries 1–7). With ML as substrate, the results for 2 are somewhat comparable to those reported for other hybrid catalysts (entries 8–12). With LIM as substrate, the catalytic results at 6 h for 2 (97% epoxides yield, entry 13) are superior to those for other hybrid catalysts (entries 13–18). At higher reaction temperature and time (75 °C, 24 h), (DMA)[MoO₃(Hbpd)] led to quantitative yield of epoxides (entry 18), although this hybrid acted as a homogeneous catalyst [63]. Another organo-oxomolybdenum compound that has been studied with biobased olefins is the polyoxometalate (POM) (Hptz)₄[SiMo₁₂O₄₀]·nH₂O, which was active

for the reactions of LIM and FAMES, but it was a homogeneous catalyst and promoted considerable epoxide ring opening reactions for the reaction systems of ML and LIM [20].

Table 2. Comparison of the catalytic results for **2** with literature data for polymeric hybrids of the type $[\text{MoO}_3(\text{L})_x]$ tested for the epoxidation of the biobased olefins and oxidation of sulfides with TBHP.

Entry	Olefin	Catalyst ^a	CB ^b	S/T ^c	Mo:Su:Ox ^d	t/h	χ (%) ^e	S _p (%) ^f	Y _p (%) ^f	Ref.
1	MO	2	HE	TFT/70	1:100:210	6/24	90/96	100/100	90/96	This work
2		[MoO ₃ (Hptz)]	HE	TFT/70	1:100:210	5/24	85/100	100/100	85/100	[19]
3		[MoO ₃ (pbim)]	HO	TFT/70	1:100:153	6/24	46/69	59/61	27/42	[37]
4		[MoO ₃ (biim)]·H ₂ O	HE	TFT/70	1:100:226	6/24	72/97	99/97	71/94	[44]
5		[MoO ₃ (bipy)]	HO	TFT/70	1:100:226	6/24	62/96	100/100	62/96	[44]
6		[MoO ₃ (bipy)]	HO	DCE/75	1:100:152	6/24	82/99	100/100	82/99	[62]
7		(DMA)[MoO ₃ (HbpdC)]	HO	TFT/75	1:103:160	6/24	93/100	98/98	91/98	[63]
8	ML	2	HE	TFT/70	1:100:210	6/24	68/88	100/97	68/85	This work
9		[MoO ₃ (Hptz)]	HE	TFT/70	1:100:210	5/24	67/86	100/98	67/84	[19]
10		[MoO ₃ (pbim)]	HO	TFT/70	1:100:153	6/24	59/92	92/77	54/71	[37]
11		[MoO ₃ (biim)]·H ₂ O	HE	TFT/70	1:100:226	6/24	66/88	100/99	66/87	[44]
12		[MoO ₃ (bipy)]	HO	TFT/70	1:100:226	6/24	63/85	100/100	63/85	[44]
13	LIM	2	HE	TFT/70	1:100:210	6	100	97	97	This work
14		[MoO ₃ (Hptz)]	HE	TFT/70	1:100:210	5/24	100/100	93/64	95/66	[19]
15		[MoO ₃ (pbim)]	HO	TFT/70	1:100:153	6/24	69/91	93/95	64/87	[37]
16		[MoO ₃ (biim)]·H ₂ O	HE	TFT/70	1:100:226	6/24	97/100	92/90	89/90	[44]
17		[MoO ₃ (bipy)]	HO	TFT/70	1:100:226	6/24	75/92	100/90	75/83	[44]
18		(DMA)[MoO ₃ (HbpdC)]	HO	TFT/75	1:103:160	6/24	95/100	100/100	95/100	[63]
19	MPS	2	HE	TFT/35	1:100:220	6/24	100/100	23/86	23/86	This work
20		[MoO ₃ (biim)]·H ₂ O	HE	TFT/35	1:100:226	6/24	100/100	7/33	7/33	[44]
21		[MoO ₃ (bipy)]	HO	DCM/20	1:100:300	4	100	traces	traces	[45]
22	DPS	2	HE	TFT/35	1:100:220	6/24	100/100	33/77	33/77	This work
23		[MoO ₃ (biim)]·H ₂ O	HE	TFT/35	1:100:226	6	100	20	20	[44]
24		[MoO ₃ (bipy)]	HO	TFT/35	1:100:226	6	100	30	30	[44]

^a Abbreviations: Hptz = 5-(2-pyridyl)tetrazole; pbim = 2-(2-pyridyl)-benzimidazole; biim = 2,2'-biimidazole; bipy = 2,2'-bipyridine; DMA = dimethylammonium; H₂bpdC = 2,2'-bipyridine-5,5'-dicarboxylic acid. ^b Catalyst behavior (HO = homogeneous catalyst (sometimes an apparent heterogeneous catalytic contribution existed), HE = heterogeneous catalyst). ^c S = solvent (TFT = α,α,α -trifluorotoluene, DCE = 1,2-dichloroethane, DCM = dichloromethane), T = reaction temperature (°C). ^d Initial molybdenum:substrate:oxidant molar ratio. ^e Substrate conversion. ^f Product selectivity (S_p) and yield (Y_p) (monoepoxide for MO; monoepoxide plus diepoxide for ML and LIM; sulfone for sulfides).

2.2.3. Sulfoxidation Activity of **2**

The catalytic applications of **2** are not restricted to olefin epoxidation. It is also an effective catalyst for the oxidation of sulfides such as methylphenylsulfide (MPS) and diphenylsulfide (DPS) with TBHP, at 35 °C (Table 1), leading to complete conversion of MPS and DPS at 1 h and 2 h, respectively. Without a catalyst, only 20% MPS and 26% DPS were converted at 4 h. The main products were the corresponding sulfoxides and sulfones. Increasing the reaction time favored the conversion of sulfoxides to sulfones, which were formed in 86% and 77% yield at 100% conversion of MPS and DPS, respectively, at 24 h (Figure 10). The main use of diphenyl sulfone is as a high boiling solvent (b.p. 379 °C) for polymerization reactions, e.g., to synthesize microporous cyanate resins [64], and high molecular weight polymers such as polyetherimides [65]. Another use of diphenyl sulfone is as a starting material for the synthesis of 3,3'-diaminodiphenyl sulfone (via the reduction of the intermediate 3,3'-dinitrodiphenyl sulfone), which has been used as a curing agent of epoxy resins [66], and a diamino monomer for the synthesis of polyimides [67]. The main use of methyl phenyl sulfone is as a starting material in organic synthesis, e.g., for the preparation of unsymmetric triarylmethanes [68].

According to the literature for oxomolybdenum catalysts, the sulfoxidation mechanism may involve a proton transfer step from the hydroperoxide oxidant to a Mo=O group of the catalyst, forming an oxidizing hydroperoxomolybdenum species (possessing the moiety {Mo(-O_αO_βH)(-OH)}) [69]. The interaction between the O_α atom and the sulfur atom of the sulfide substrate results in O_β-O_α bond rupture and formation of a S=O bond (leading to the sulfoxide; or of the sulfoxide intermediate, leading to the sulfone).

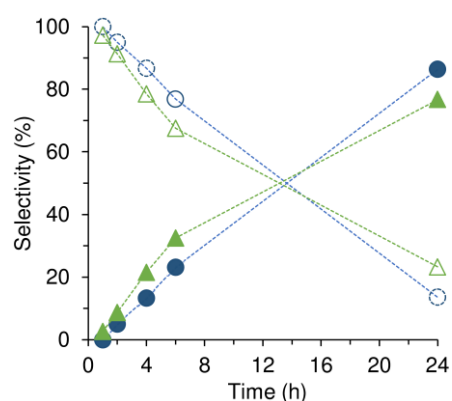


Figure 10. Selectivity of sulfoxides (○,△) and sulfones (●,▲) for reactions of MPS (○,●) and DPS (△,▲) as a function of time using **2** as catalyst and TBHP as oxidant, at 35 °C. Dashed lines are visual guides.

Catalyst **2** is one of the few $[\text{MoO}_3(\text{L})_x]$ -type catalysts tested for the studied sulfoxidation reactions (Table 2). Under similar reaction conditions, **2** and the hybrids $[\text{MoO}_3\text{L}]$ with $\text{L} = \text{bipy}$ or biim led to complete conversion of DPS with TBHP at 6 h and sulfone yields of 20–33% (entries 22–24, Table 2) [44]. With MPS as substrate, **2** was more effective for sulfone production than $[\text{MoO}_3(\text{biim})] \cdot \text{H}_2\text{O}$: 86% vs. 33% sulfone yield at 24 h (100% conversion) (entries 19 and 20, Table 2) [44]. Under different reaction conditions, $[\text{MoO}_3(\text{bipy})]$ led to 94% sulfoxide yield at 4 h and 20 °C (dichloromethane as solvent, initial Mo:sulfide:TBHP molar ratio = 1:100:300) [45].

3. Materials and Methods

3.1. Reagents and Chemicals

The following reagents and chemicals were purchased from Sigma-Aldrich (St. Louis, MO, USA), unless otherwise stated, and used as received: (for the preparation of 5-(2-pyridyl)tetrazole) 2-cyanopyridine, acetic acid, sodium azide, butanol, and hydrochloric acid; (for the preparation of 5-(2-pyridyl-1-oxide)tetrazole (Hpto)) methanol ($\geq 99.8\%$), 3-chloroperoxybenzoic acid (Acros Organics, Thermo Fisher Scientific, Geel, Belgium, 70–75%); (for the synthesis of compounds **2** and **3**) molybdenum(VI) dichloride dioxide, anhydrous tetrahydrofuran ($\geq 99.9\%$), hexane ($\geq 99\%$, Carlo Erba, Milan, Italy), anhydrous diethyl ether (Honeywell, $\geq 99.8\%$), and acetone (Honeywell, $\geq 99.5\%$); (for the catalytic reactions) *cis*-cyclooctene (95%, Alfa Aesar, Ward Hill, MA, USA), methyl oleate (99%), methyl linoleate (95%, Alfa Aesar, Ward Hill, MA, USA), methyl linolenate (98.5%, Acros Organics), methyl ricinoleate ($\geq 99\%$), *dl*-limonene ($>95\%$, Merck, Kenilworth, NJ, USA), methyl phenyl sulfide (99%), diphenyl sulfide (98%), *tert*-butyl hydroperoxide (5.5 M in decane, containing $<4\%$ water), 30% aq. hydrogen peroxide, anhydrous α, α, α -trifluorotoluene ($\geq 99\%$), acetone (99.5%, Honeywell, Riedel de Haen, Seelze, Germany), and acetonitrile (99.9%, Panreac, Barcelona, Spain); (for sample preparation for GC analysis) 1,2-dichloroethane ($\geq 99\%$), ethyl decanoate (99%), undecane ($>99\%$), and mesitylene (98%).

3.2. Instrumentation

Elemental analyses (carbon, hydrogen, and nitrogen) were performed using a Leco TruSpec 630-200-200 analyzer (Leco, Saint Joseph, MI, USA). ICP-OES analyses (for Mo) were performed at the Central Analysis Laboratory (University of Aveiro); the measurements were carried out on a Horiba JobinYvon Activa M spectrometer (Horiba Scientific, Palaiseau, France). Prior to analyses, the solid samples were digested using 1 mL HF and 1 mL HNO₃, and microwave heating at 180 °C. Powder X-Ray diffraction (PXRD) data were collected on a Malvern Panalytical (Malvern, UK) Empyrean diffractometer (Cu-K α X-radiation, $\lambda = 1.54060 \text{ \AA}$) in a Bragg-Brentano para-focusing optics configuration (45 kV, 40 mA) at ambient temperature. Samples were prepared in a spinning flat plate sample holder and step-scanned from 3 to 70° (2θ) in 0.02° 2θ steps with a counting time of 50 s

per step. SEM images, elemental mappings (Mo), and EDS analyses were obtained on a Hitachi SU-70 SEM microscope (Hitachi High-Tech Europe GmbH, Krefeld, Germany) with a Bruker Quantax 400 detector operating at 15 kV (Bruker, Billerica, MA, USA). Samples were prepared by deposition on aluminium sample holders followed by carbon coating using an Emitech K950 carbon evaporator (Emitech SAS, Montigny-le-Bretonnex, France). The textural properties of **2** were determined from the N₂ sorption isotherm at −196 °C, which was measured using a Quantachrome instrument (automated gas sorption data using Autosorb IQ2, Quantachrome Instruments, Florida, USA). The sample was pre-treated at 60 °C for 8 h, under vacuum ($<4 \times 10^{-3}$ bar). The specific surface area was calculated using the Brunauer, Emmett, Teller equation (S_{BET}) and the total pore volume (V_p) was based on the Gurvitch rule (for relative pressure (p/p_0) of 0.996). The pore size distribution was calculated from the adsorption branch by the Barrett–Joyner–Halenda (BJH) method. Fourier transform infrared (FT-IR) spectra (in the range of 4000–350 cm^{−1}) were measured on a Bruker Tensor 27 spectrophotometer (resolution 4 cm^{−1}, 128 scans, Bruker, Billerica, MA, USA) as KBr pellets. Attenuated total reflectance (ATR) FT-IR spectra were measured on the same instrument equipped with a Specac[®] Golden Gate Mk II ATR accessory (Specac, Orpington, UK) having a diamond top plate and KRS-5 focusing lenses. FT-Raman spectra were recorded on a Bruker MultiRAM spectrometer equipped with a Nd:YAG laser with an excitation wavelength of 1064 nm (Bruker, Billerica, MA, USA). Solution ¹H and ¹³C NMR spectra were recorded with a Bruker Avance 300 spectrometer using DMSO-*d*₆ as a solvent. ¹H-¹³C HSQC NMR experiments were performed on a 500 MHz JEOL system equipped with a Royal HFX probe. The ¹³C{¹H} cross-polarization (CP) magic-angle spinning (MAS) NMR spectra were recorded using a Bruker Avance 400 spectrometer with an ultra-shielded static magnetic field of 100.6 MHz with 3.2 μs pulses, 3.5 ms contact time, spinning rate of 12 kHz, and 5 s recycle delays (NMR, Bruker, Billerica, MA, USA).

3.3. Synthesis

All preparations and manipulations were performed using standard Schlenk techniques under an inert atmosphere. For the preparation of 5-(2-pyridyl)tetrazole (Hptz), the method reported by McManus and Herbst was followed without any further modification [70].

3.3.1. 5-(2-pyridyl-1-oxide)tetrazole (Hpto)

The procedure described by Pietraszkiewicz et al. was followed to prepare the ligand Hpto [27]. 3-Chloroperoxybenzoic acid (1.39 g, 8.05 mmol) was added slowly to a colorless solution of Hptz (0.47 g, 3.20 mmol) in methanol (48 mL). After stirring the mixture at room temperature for 48 h, the resultant white precipitate was isolated by filtration, washed with methanol (3 × 20 mL), and vacuum-dried. Yield: 0.37 g, 71%. Single crystals of Hpto suitable for XRD were obtained by slow evaporation of the mother-liquor. Anal. Calcd for C₆H₅N₅O (163.14): C, 44.17; H, 3.09; N, 42.93. Found: C, 44.34; H, 3.23; N, 42.78%. FT-IR (KBr, cm^{−1}): $\nu = 3107$ (w), 1654 (w), 1465 (m), 1453 (s), 1384 (m), 1337 (w), 1267 (m), 1245 (m), 1224 (m), 1197 (m), 1154 (w), 1111 (m), 1094 (w), 1069 (m), 1016 (m), 842 (m), 778 (s), 754 (m), 719 (w), 698 (m), 573 (w), 553 (m), 480 (w), 399 (w). Raman (cm^{−1}): $\nu = 3107$ (w), 3092 (w), 3061 (w), 1614 (m), 1571 (m), 1538 (m), 1466 (w), 1382 (w), 1324 (w), 1274 (w), 1248 (w), 1227 (w), 1165 (m), 1111 (w), 1062 (w), 1042 (w), 1008 (w), 962 (w), 841 (m), 788 (w), 755 (w), 719 (w), 687 (w), 578 (w), 553 (w), 482 (w), 373 (w), 345 (w), 324 (w), 239 (w), 182 (w), 125 (m), 79 (vs). ¹H NMR (300.13 MHz, 25 °C, DMSO-*d*₆): $\delta = 8.55$ (dd, $J_{\text{H-H}} = 6.5, 1.1$ Hz, 1H, H6), 8.41 (dd, $J_{\text{H-H}} = 7.8, 2.1$ Hz, 1H, H3), 7.66 (dt, $J_{\text{H-H}} = 7.8, 2.1$ Hz, 1H, H5), 7.60 (t, $J_{\text{H-H}} = 6.5$ Hz, 1H, H4) ppm. ¹³C{¹H} NMR (75.47 MHz, 25 °C, DMSO-*d*₆): $\delta = 147.8$ (Ctz), 140.2 (C6), 134.7 (C2), 128.3 (C5), 126.8 (C3), 126.5 (C4) ppm. ¹³C{¹H} CP MAS NMR: $\delta = 146.2$ (Ctz), 142.0 (C6), 133.4 (C2), 127.9 (C3, C4 and C5) ppm.

3.3.2. [MoO₂Cl₂(Hpto)]·THF (1)

Anhydrous THF (20 mL) was added to MoO₂Cl₂ (0.50 g, 2.51 mmol) and the mixture was stirred at 50 °C for 20 min. Next, the ligand Hpto (0.41 g, 2.51 mmol) was added and the reaction mixture was left to stir at room temperature for 2 h. Complex **1** was isolated by filtration, washed with diethyl ether (2 × 10 mL), and vacuum-dried. Yield: 0.64 g, 59%. Single crystals of **1** suitable for XRD were obtained by slow diffusion of anhydrous diethyl ether into a solution of **1** in anhydrous THF. Anal. Calcd for C₁₀H₁₃Cl₂MoN₅O₄ (434.09): C, 27.67; H, 3.02; N, 16.13. Found: C, 28.00, H, 3.00, N, 16.65%. FT-IR (KBr, cm⁻¹): ν = 3399 (w), 1634 (w), 1530 (w), 1455 (s), 1385 (w), 1268 (w), 1246 (w), 1218 (m), 1149 (w), 1110 (w), 1054 (w), 1038 (w), 1013 (w), 945 (s), 909 (s), 841 (m), 779 (s), 757 (s), 713 (w), 696 (w), 595 (w), 573 (w), 395 (m). Raman (cm⁻¹): ν = 3094 (w), 2895 (w), 1794 (w), 1620 (s), 1582 (m), 1536 (m), 1449 (m), 1324 (w), 1273 (w), 1247 (w), 1217 (w), 1163 (w), 1107 (w), 1040 (w), 1012 (w), 946 (s), 913 (m), 849 (w), 819 (w), 693 (w), 602 (w), 575 (w), 491 (w), 400 (w), 312 (w), 287 (w), 252 (w), 228 (m), 213 (m), 191 (w), 138 (w), 77 (vs). ¹³C{¹H} CP MAS NMR: δ = 154.1 (Ctz), 140.4 (C6), 137.0 (C2 and C4), 129.2 (C3 or C5), 128.2 (C3 or C5), 69.4 (C_{THF}), 26.5 (C_{THF}) ppm.

3.3.3. [MoO₃(Hpto)]·H₂O (2)

Milli-Q water (20 mL) was added to **1** (0.40 g, 0.92 mmol), and the mixture was refluxed for 16 h. A white precipitate suspended in a colorless solution (pH = 1-2) was obtained. The solid (**2**) was isolated by filtration; washed with distilled water (2 × 10 mL), acetone (2 × 10 mL), and diethyl ether (2 × 10 mL); and vacuum-dried. Yield: 0.19 g, 67%. Anal. Calcd for C₆H₅MoN₅O₄·H₂O (325.09): C, 22.17; H, 2.17; N, 21.54; Mo, 29.5. Found: C, 22.29; H, 2.07; N, 21.65; Mo, 29.5%. FT-IR (KBr, cm⁻¹): ν = 3356 (m), 3084 (w), 3034 (w), 1874 (w), 1633 (m), 1572 (w), 1529 (w), 1455 (vs), 1386 (m), 1280 (w), 1246 (w), 1213 (s), 1185 (w), 1158 (w), 1120 (w), 1108 (w), 1084 (m), 1032 (m), 1014 (w), 974 (w), 941 (s), 908 (sh), 898 (vs), 840 (s), 791 (w), 759 (m), 713 (w), 694 (w), 593 (m), 573 (w), 523 (w), 499 (w), 436 (w), 396 (m). Raman (cm⁻¹): ν = 3091 (w), 3050 (w), 3036 (w), 1620 (s), 1573 (w), 1530 (m), 1448 (m), 1386 (w), 1247 (w), 1210 (w), 1187 (w), 1159 (w), 1120 (w), 1109 (w), 1087 (w), 1052 (w), 1032 (w), 1015 (w), 937 (vs), 906 (m), 895 (s), 840 (w), 795 (w), 764 (w), 723 (w), 694 (w), 594 (w), 571 (w), 530 (w), 503 (w), 403 (w), 374 (w), 340 (w), 303 (w), 246 (w), 213 (w), 183 (w), 143 (s), 120 (w), 104 (w), 78 (vs), 64 (vs). ¹³C{¹H} CP MAS NMR: δ = 151.9 (Ctz), 138.5 (C2 and C6), 135.8 (C4), 128.8 (C3 and C5) ppm.

3.4. Catalytic Tests

The catalytic reactions of *cis*-cyclooctene (Cy8), biomass-derived olefins and sulfides were carried out at 35 or 70 °C, using 1.8 mmol of substrate, cosolvent (1 mL), catalyst (in an amount equivalent to 18 μ mol of Mo), and *tert*-butyl hydroperoxide (TBHP) or H₂O₂ as oxidant.

The reactions with TBHP (2.75 mmol oxidant for Cy8; 3.85 mmol for biobased olefins or sulfides) were carried out using 10 mL borosilicate reactors equipped with a Teflon valve for sampling and a PTFE-coated magnetic stirring bar. Initially, catalyst, solvent, and substrate were added to the reactor, which was then immersed in a temperature-controlled oil bath at 70 °C under stirring (1000 rpm). After 10 min, preheated TBHP was added to the reactor, and this moment was taken as the initial instant of the catalytic reaction.

The reactions with H₂O₂ (2.75 mmol) were performed in tubular borosilicate batch reactors with pear-shaped bottoms (*ca.* 12 mL capacity), equipped with an appropriate PTFE-coated magnetic stirring bar (for stirring at 1000 rpm) and a valve. Catalyst, substrate, solvent, and H₂O₂ were loaded into the reactor, which was then immersed in a thermostatically controlled oil bath (70 °C), and this moment was considered as the initial instant of the catalytic reaction.

The evolution of the reactions was monitored by analyzing freshly prepared samples by gas chromatography (GC), using a Varian 450 GC instrument equipped with a BR-5 capillary column (30 m × 0.25 mm × 0.25 μ m) and an FID detector with H₂ as carrier gas.

The products were identified using pure compounds and/or GC-MS, using a GC-2010 Plus (Shimadzu) and a GCMS-QP2010 Ultra (Shimadzu), equipped with a ZB-5ms column (He as carrier gas). The quantification of reactants/products was based on calibrations. For the sets of substrates Cy8/LIM, MO/ML/MLN/MR, and MPS/DPS, the internal standards used were undecane, methyl decanoate, and mesitylene, respectively.

The catalyst stability was evaluated by reusing the recovered solids in consecutive batch runs, keeping constant the initial mass ratio of catalyst: Cy8:TBHP between runs (the solids were denoted *i*-used, *i* = 1 or 2). After each run, the solids were separated from the reaction mixture by centrifugation (3500 rpm), thoroughly washed with acetone, dried overnight under atmospheric conditions, and finally vacuum-dried (*ca.* 0.1 bar) at 60 °C for 1 h. The obtained solids were characterized by ATR FT-IR spectroscopy, PXRD, and/or SEM/mapping. A leaching test was performed to verify whether soluble active species were present in the liquid phase for the systems 1/Cy8/TBHP/TFT, at 55 °C, and 2/Cy8/TBHP/TFT, at 70 °C, under identical conditions to those used for a typical batch run. Specifically, at 0.5 h for 1, and 1 h for 2, the hot solid–liquid biphasic mixture was filtered through a 0.2 µm PTFE membrane filter, and the filtrate was transferred to a separate stirred reactor (preheated at 55 or 70 °C), and the evolution of the obtained solution was monitored by GC.

4. Conclusions

A polymeric hybrid molybdenum oxide/organic catalyst, [MoO₃(Hpto)]·H₂O, was synthesized by a simple, neat strategy from [MoO₂Cl₂(Hpto)]·THF, and the spectroscopic characterization indicated that the ligand 5-(2-pyridyl-1-oxide)tetrazole was involved in bidentate N,O-coordination to Mo^{VI} centers in both the precursor complex and the hybrid derivative. The two compounds were compared as olefin epoxidation catalysts, being very active and selective toward the formation of epoxide products. The mononuclear complex and the polymeric hybrid present different catalytic features. While the precursor acts as a homogeneous catalyst, the hybrid is one of the rare examples among molybdenum oxide/organic catalysts that acts as a solid catalyst. The hybrid may be used not only for olefin epoxidation with a broad substrate scope (covering bioderived olefins such as FAMES and terpenes), but also for other reactions such as sulfoxidations under mild conditions, which were selective toward sulfone products. Epoxide yields at 24 h were in the range of 96–100% for methyl oleate and methyl ricinoleate, and 85–92% (total epoxides) for polyenes, namely *dl*-limonene, methyl linoleate, and methyl linolenate. On the other hand, sulfone yields were in the range of 77–86% at 24 h. For the first time, in this work, a molybdenum-based catalyst was applied for methyl linolenate epoxidation, and methyl ricinoleate epoxidation was demonstrated using a [MoO₃(L)_x]-type hybrid catalyst. Future work will aim at developing alternative synthesis routes to 2 and resolving its structure.

Supplementary Materials: The following supporting information can be downloaded at: <https://www.mdpi.com/article/10.3390/catal13030565/s1>, Figure S1: ¹H-¹³C HSQC NMR spectrum of Hpto in DMSO-*d*₆; Figure S2: N₂ sorption isotherm and pore size distribution of 2; Experimental details for the single-crystal X-ray diffraction studies; Table S1: Hydrogen-bonding geometry for Hpto; Table S2: Hydrogen-bonding geometry for compound [MoO₂Cl₂(Hpto)]·THF (1); Table S3: Crystal data and structure refinement details for the organic ligand Hpto and complex [MoO₂Cl₂(Hpto)]·THF (1); Refs [71–79] are cited in the Supplementary Material file.

Author Contributions: Conceptualization, A.A.V., I.S.G. and M.P.; validation, A.C.G., P.N., F.A.A.P., A.A.V., I.S.G. and M.P.; investigation, M.S.N., D.M.G., A.C.G., P.N., R.F.M. and A.D.L.; resources, F.A.A.P., A.A.V., I.S.G. and M.P.; writing—original draft preparation, M.S.N., D.M.G., A.C.G., P.N., R.F.M. and A.D.L.; writing—review and editing, F.A.A.P., A.A.V. and M.P.; visualization, M.S.N., D.M.G., A.C.G., P.N., R.F.M., A.A.V., I.S.G. and M.P.; supervision, P.N., F.A.A.P., A.A.V., I.S.G. and M.P.; project administration, P.N., A.A.V. and I.S.G.; funding acquisition, P.N. and A.A.V. All authors have read and agreed to the published version of the manuscript.

Funding: This work was carried out with the support of CICECO—Aveiro Institute of Materials (FCT (Fundação para a Ciência e a Tecnologia) ref. UIDB/50011/2020, UIDP/50011/2020 and LA/P/0006/2020) and the COMPETE 2020 Operational Thematic Program for Competitiveness and Internationalization (Project POCI-01-0145-FEDER-030075), co-financed by national funds through the FCT/MCTES (PIDDAC) and the European Union through the European Regional Development Fund under the Portugal 2020 Partnership Agreement. This study received Portuguese national funds from the FCT through the operational programs CRESCE Algarve 2020 and COMPETE 2020 through project EMBRC.PT ALG-01-0145-FEDER-022121. M.S.N. (grant ref. 2021.06403.BD) and D.M.G. (grant ref. 2021.04756.BD) acknowledge the FCT for Ph.D. grants (State Budget, European Social Fund (ESF) within the framework of PORTUGAL2020, namely through the Centro 2020 Regional Operational Program). A.C.G. (CEECIND/02128/2017) and R.F.M. (CEECIND/00553/2017) thank the FCT/MCTES for funding through the Individual Call to Scientific Employment Stimulus.

Data Availability Statement: Data are contained within the article or Supplementary Materials.

Conflicts of Interest: The authors declare no conflict of interest. The funders had no role in the design of the study; in the collection, analyses, or interpretation of data; in the writing of the manuscript; or in the decision to publish the results.

References

1. Neochoritis, C.G.; Zhao, T.; Dömling, A. Tetrazoles via Multicomponent Reactions. *Chem. Rev.* **2019**, *119*, 1970–2042. [[CrossRef](#)] [[PubMed](#)]
2. Massi, M.; Stagni, S.; Ogden, M.I. Lanthanoid Tetrazole Coordination Complexes. *Coord. Chem. Rev.* **2018**, *375*, 164–172. [[CrossRef](#)]
3. Bhatt, U. Five-Membered Heterocycles with Four Heteroatoms: Tetrazoles. In *Modern Heterocyclic Chemistry*; Alvarez-Builla, J., Vaquero, J.J., Barluenga, J., Eds.; Wiley-VCH Verlag & Co. KGaA: Weinheim, Germany, 2011; pp. 1401–1430.
4. Nasrollahzadeh, M.; Nezafat, Z.; Bidgoli, N.S.S.; Shafiei, N. Use of Tetrazoles in Catalysis and Energetic Applications: Recent Developments. *Mol. Catal.* **2021**, *513*, 111788. [[CrossRef](#)]
5. Wang, X.-S.; Tang, Y.-Z.; Huang, X.-F.; Qu, Z.-R.; Che, C.-M.; Chan, P.W.H.; Xiong, R.-G. Syntheses, Crystal Structures, and Luminescent Properties of Three Novel Zinc Coordination Polymers with Tetrazolyl Ligands. *Inorg. Chem.* **2005**, *44*, 5278–5285. [[CrossRef](#)] [[PubMed](#)]
6. Malik, M.A.; Wani, M.Y.; Al-Thabaiti, S.A.; Shiekh, R.A. Tetrazoles as carboxylic acid isosteres: Chemistry and biology. *J. Incl. Phenom. Macrocycl. Chem.* **2014**, *78*, 15–37. [[CrossRef](#)]
7. Wang, T.; Gao, H.; Shreeve, J.M. Functionalized Tetrazole Energetics: A Route to Enhanced Performance. *Z. Anorg. Allg. Chem.* **2021**, *647*, 157–191. [[CrossRef](#)]
8. Go, M.J.; Lee, K.M.; Oh, C.H.; Kang, Y.Y.; Kim, S.H.; Park, H.R.; Kim, Y.; Lee, J. New Titanium Catalysts Containing Tetrazole for Cycloaddition of CO₂ to Epoxides. *Organometallics* **2013**, *32*, 4452–4455. [[CrossRef](#)]
9. Frija, L.M.T.; Alegria, E.C.B.A.; Sutradhar, M.; Cristiano, M.L.S.; Ismael, A.; Kopylovich, M.N.; Pombeiro, A.J.L. Copper(II) and cobalt(II) tetrazole-saccharinate complexes as effective catalysts for oxidation of secondary alcohols. *J. Mol. Catal. A Chem.* **2016**, *425*, 283–290. [[CrossRef](#)]
10. Kumari, J.; Mobin, S.M.; Mukhopadhyay, S.; Vyas, K.M. Efficient oxidation of benzene catalyzed by Cu(II) tetrazolato complexes under mild conditions. *Inorg. Chem. Commun.* **2019**, *105*, 217–220. [[CrossRef](#)]
11. Sajjadi, M.; Nasrollahzadeh, M.; Ghafuri, H. Cu(II)-N-Benzyl-Amino-1H-Tetrazole Complex Immobilized on Magnetic Chitosan as a Highly Effective Nanocatalyst for C-N Coupling Reactions. *J. Organomet. Chem.* **2021**, *950*, 121959. [[CrossRef](#)]
12. Ariannezhad, M.; Habibi, D.; Heydari, S.; Khorramabadi, V. The capable Pd complex immobilized on the functionalized polymeric scaffold for the green benzylation reaction. *Appl. Organomet. Chem.* **2021**, *35*, e6208. [[CrossRef](#)]
13. He, Y.; Cai, C. Tetrazole Functionalized Polymer Supported Palladium Complex: An Efficient and Reusable Catalyst for the Room-Temperature Suzuki Cross-Coupling Reaction. *Catal. Lett.* **2010**, *40*, 153–159. [[CrossRef](#)]
14. Mrowiec, A.; Jurowska, A.; Hodorowicz, M.; Szklarzewicz, J. 5-(2-Pyridyl)-1H-Tetrazole Complexes with Mo(IV) and W(IV) Cyanides. *Dalton Trans.* **2017**, *46*, 4030–4037. [[CrossRef](#)] [[PubMed](#)]
15. Wu, X.-Y.; Zhang, Q.-K.; Kuang, X.-F.; Yang, W.; Yu, R.-M.; Lu, C.-Z. Two Hybrid Polyoxometalate-Pillared Metal–Organic Frameworks. *Dalton Trans.* **2012**, *41*, 11783–11787. [[CrossRef](#)] [[PubMed](#)]
16. Liu, M.-g.; Zhang, P.-p.; Peng, J.; Meng, H.-x.; Wang, X.; Zhu, M.; Wang, D.-d.; Meng, C.-l.; Alimaje, K. Organic–Inorganic Hybrids Constructed from Mixed-Valence Multinuclear Copper Complexes and Templated by Keggin Polyoxometalates. *Cryst. Growth Des.* **2012**, *12*, 1273–1281. [[CrossRef](#)]
17. Darling, K.; Ouellette, W.; Prosvirin, A.; Freund, S.; Dunbar, K.R.; Zubieta, J. Solid State Coordination Chemistry of the Copper(II)/Pyridyl- and Pyrazine-Tetrazolate/Sulfate System. *Cryst. Growth Des.* **2012**, *12*, 2662–2672. [[CrossRef](#)]
18. Gaponik, P.N.; Voitekhovich, S.V.; Ivashkevich, O.A. Metal Derivatives of Tetrazoles. *Russ. Chem. Rev.* **2006**, *75*, 507–539. [[CrossRef](#)]

19. Nunes, M.S.; Gomes, D.M.; Gomes, A.C.; Neves, P.; Mendes, R.F.; Almeida Paz, F.A.; Lopes, A.D.; Valente, A.A.; Gonçalves, I.S.; Pillinger, M. A 5-(2-Pyridyl)Tetrazolate Complex of Molybdenum(VI), Its Structure, and Transformation to a Molybdenum Oxide-Based Hybrid Heterogeneous Catalyst for the Epoxidation of Olefins. *Catalysts* **2021**, *11*, 1407. [[CrossRef](#)]
20. Nunes, M.S.; Neves, P.; Gomes, A.C.; Cunha-Silva, L.; Lopes, A.D.; Valente, A.A.; Pillinger, M.; Gonçalves, I.S. A Silicododecamolybdate/Pyridinium-Tetrazole Hybrid Molecular Salt as a Catalyst for the Epoxidation of Bio-Derived Olefins. *Inorg. Chim. Acta* **2021**, *516*, 120129. [[CrossRef](#)]
21. Yan, W.; Wang, Z.; Luo, C.; Xia, X.; Liu, Z.; Zhao, Y.; Du, F.; Jin, X. Opportunities and Emerging Challenges of the Heterogeneous Metal-Based Catalysts for Vegetable Oil Epoxidation. *ACS Sustain. Chem. Eng.* **2022**, *10*, 7426–7446. [[CrossRef](#)]
22. Moser, B.R.; Cermak, S.C.; Doll, K.M.; Kenar, J.A.; Sharma, B.K. A review of fatty epoxide ring opening reactions: Chemistry, recent advances, and applications. *J. Am. Oil Chem. Soc.* **2022**, *99*, 801–842. [[CrossRef](#)]
23. Monica, F.D.; Kleij, A.W. From Terpenes to Sustainable and Functional Polymers. *Polym. Chem.* **2020**, *11*, 5109–5127. [[CrossRef](#)]
24. Chen, T.C.; da Fonseca, C.O.; Schönthal, A.H. Preclinical Development and Clinical Use of Perillyl Alcohol for Chemoprevention and Cancer Therapy. *Am. J. Cancer Res.* **2015**, *5*, 1580–1593.
25. Cardoso De Almeida, A.A.; Silva, R.O.; Duarte Nicolau, L.A.; Vieira De Brito, T.; Pergentino de Sousa, D.; dos Reis Barbosa, A.L.; Mendes De Freitas, R.; da Silva Lopes, L.; Medeiros, J.-V.R.; Ferreira, P.M.P. Physio-Pharmacological Investigations About the Anti-Inflammatory and Antinociceptive Efficacy of (+)-Limonene Epoxide. *Inflammation* **2017**, *40*, 511–522. [[CrossRef](#)] [[PubMed](#)]
26. Facchetti, A.; Abbotto, A.; Beverina, L.; Bradamante, S.; Mariani, P.; Stern, C.L.; Marks, T.J.; Vacca, A.; Pagani, G.A. Novel Coordinating Motifs for Lanthanide(III) Ions Based on 5-(2-Pyridyl)Tetrazole and 5-(2-Pyridyl-1-Oxide)Tetrazole. Potential New Contrast Agents. *Chem. Commun.* **2004**, 1770–1771. [[CrossRef](#)] [[PubMed](#)]
27. Pietraszkiewicz, M.; Mal, S.; Pietraszkiewicz, O. Novel, Highly Photoluminescent Eu(III) and Tb(III) Tetrazolate-2-Pyridine-1-Oxide Complexes. *Opt. Mater.* **2012**, *34*, 1507–1512. [[CrossRef](#)]
28. Mal, S.; Pietraszkiewicz, M.; Pietraszkiewicz, O. Synthesis and Photophysical Studies of Tetrazolate-Based Eu(III) Photoluminescent Ternary Complexes Containing N-Heterocyclic Phosphine Oxides Auxiliary Co-Ligands. *Luminescence* **2016**, *31*, 1085–1090. [[CrossRef](#)]
29. Gao, F.; Yao, C.-S.; Lu, Z.-S.; Shi, Y.-H. Diaquabis[5-(1-Oxidopyridin-1-ium-2-yl)-1,2,3,4-Tetrazolido]Manganese(II) Dihydrate. *Acta Crystallogr. E Crystallogr. Commun.* **2011**, *67*, m213. [[CrossRef](#)]
30. Groom, C.R.; Bruno, I.J.; Lightfoot, M.P.; Ward, S.C. The Cambridge Structural Database. *Acta Crystallogr. B Struct. Sci. Cryst. Eng. Mater.* **2016**, *72*, 171–179. [[CrossRef](#)]
31. Kühn, F.E.; Lopes, A.D.; Santos, A.M.; Herdtweck, E.; Haider, J.J.; Romão, C.C.; Santos, A.G. Lewis base adducts of bis-(halogeno)dioxomolybdenum(VI): Syntheses, structures, and catalytic applications. *J. Mol. Catal. A Chem.* **2000**, *151*, 147–160. [[CrossRef](#)]
32. Abrantes, M.; Amarante, T.R.; Antunes, M.M.; Gago, S.; Paz, F.A.A.; Margiolaki, I.; Rodrigues, A.E.; Pillinger, M.; Valente, A.A.; Gonçalves, I.S. Synthesis, structure, and catalytic performance in cyclooctene epoxidation of a molybdenum oxide/bipyridine hybrid material: $[\text{MoO}_3(\text{bipy})][\text{MoO}_3(\text{H}_2\text{O})]_n$. *Inorg. Chem.* **2010**, *49*, 6865–6873. [[CrossRef](#)] [[PubMed](#)]
33. Amarante, T.R.; Neves, P.; Tomé, C.; Abrantes, M.; Valente, A.A.; Paz, F.A.A.; Pillinger, M.; Gonçalves, I.S. An octanuclear molybdenum(VI) complex containing coordinatively bound 4,4'-di-tert-butyl-2,2'-bipyridine, $[\text{Mo}_8\text{O}_{22}(\text{OH})_4(\text{di-}t\text{Bu-bipy})_4]$: Synthesis, structure, and catalytic epoxidation of bio-derived olefins. *Inorg. Chem.* **2012**, *51*, 3666–3676. [[CrossRef](#)] [[PubMed](#)]
34. Figueiredo, S.; Gomes, A.C.; Neves, P.; Amarante, T.R.; Paz, F.A.A.; Soares, R.; Lopes, A.D.; Valente, A.A.; Pillinger, M.; Gonçalves, I.S. Synthesis, structural elucidation, and application of a pyrazolopyridine–molybdenum oxide composite as a heterogeneous catalyst for olefin epoxidation. *Inorg. Chem.* **2012**, *51*, 8629–8635. [[CrossRef](#)] [[PubMed](#)]
35. Amarante, T.R.; Neves, P.; Gomes, A.C.; Nolasco, M.; Ribeiro-Claro, P.; Coelho, A.C.; Valente, A.A.; Paz, F.A.A.; Smeets, S.; McCusker, L.B.; et al. Synthesis, structural elucidation, and catalytic properties in olefin epoxidation of the polymeric hybrid material $[\text{Mo}_3\text{O}_9(2\text{-}[3(5)\text{-pyrazolyl}]\text{pyridine})]_n$. *Inorg. Chem.* **2014**, *53*, 2652–2665. [[CrossRef](#)]
36. Amarante, T.R.; Neves, P.; Paz, F.A.A.; Valente, A.A.; Pillinger, M.; Gonçalves, I.S. Investigation of a dichlorodioxomolybdenum(VI)-pyrazolopyridine complex and a hybrid derivative as catalysts in olefin epoxidation. *Dalton Trans.* **2014**, *43*, 6059–6069. [[CrossRef](#)]
37. Neves, P.; Nogueira, L.S.; Gomes, A.C.; Oliveira, T.S.M.; Lopes, A.D.; Valente, A.A.; Gonçalves, I.S.; Pillinger, M. Chemistry and catalytic performance of pyridyl-benzimidazole oxidomolybdenum(VI) compounds in (bio)olefin epoxidation. *Eur. J. Inorg. Chem.* **2017**, *2017*, 2617–2627. [[CrossRef](#)]
38. Brégeault, J.-M. Transition-Metal Complexes for Liquid-Phase Catalytic Oxidation: Some Aspects of Industrial Reactions and of Emerging Technologies. *Dalton Trans.* **2003**, 3289–3302. [[CrossRef](#)]
39. Hub, S.; Maj, P. Manufacture of Tertiobutyl Hydroperoxyde from Renewable Materials, Tertiobutyl Hydroperoxide Thus Obtained, and Uses Thereof. U.S. Patent 8,536,379 B2, 17 September 2013.
40. Božek, B.; Neves, P.; Oszajca, M.; Valente, A.A.; Połtowicz, J.; Pamin, K.; Łasocha, W. Simple Hybrids Based on Mo or W Oxides and Diamines: Structure Determination and Catalytic Properties. *Catal. Lett.* **2020**, *150*, 713–727. [[CrossRef](#)]
41. Neves, P.; Lysenko, A.B.; Gomes, A.C.; Pillinger, M.; Gonçalves, I.S.; Valente, A.A. Behavior of Triazolylmolybdenum(VI) Oxide Hybrids as Oxidation Catalysts with Hydrogen Peroxide. *Catal. Lett.* **2017**, *147*, 1133–1143. [[CrossRef](#)]
42. Lysenko, A.B.; Senchyk, G.A.; Domasevitch, K.V.; Hauser, J.; Fuhrmann, D.; Kobalz, M.; Krautscheid, H.; Neves, P.; Valente, A.A.; Gonçalves, I.S. Synthesis and Structural Elucidation of Triazolylmolybdenum(VI) Oxide Hybrids and Their Behavior as Oxidation Catalysts. *Inorg. Chem.* **2015**, *54*, 8327–8338. [[CrossRef](#)]

43. Maul, J.J.; Ostrowski, P.J.; Ublacker, G.A.; Linclau, B.; Curran, D.P. Benzotrifluoride and Derivatives: Useful Solvents for Organic Synthesis. In *Modern Solvents in Organic Synthesis*; Knochel, P., Ed.; Springer: Berlin/Heidelberg, Germany, 1999; Volume 206, pp. 79–105.
44. Amarante, T.R.; Neves, P.; Paz, F.A.A.; Gomes, A.C.; Pillinger, M.; Valente, A.A.; Gonçalves, I.S. Heterogeneous Catalysis with an Organic–Inorganic Hybrid Based on MoO₃ Chains Decorated with 2,2′-Biimidazole Ligands. *Catal. Sci. Technol.* **2021**, *11*, 2214–2228. [[CrossRef](#)]
45. Tosi, I.; Vurchio, C.; Abrantes, M.; Gonçalves, I.S.; Pillinger, M.; Cavani, F.; Cordero, F.M.; Brandi, A. [MoO₃(2,2′-Bipy)]_n Catalyzed Oxidation of Amines and Sulfides. *Catal. Commun.* **2018**, *103*, 60–64. [[CrossRef](#)]
46. Neves, P.; Gomes, A.C.; Paz, F.A.A.; Valente, A.A.; Gonçalves, I.S.; Pillinger, M. Synthesis, Structure and Catalytic Olefin Epoxidation Activity of a Dinuclear Oxo-Bridged Oxodiperoxomolybdenum(VI) Complex Containing Coordinated 4,4′-Bipyridinium. *Mol. Catal.* **2017**, *432*, 104–114. [[CrossRef](#)]
47. Nogueira, L.S.; Neves, P.; Gomes, A.C.; Amarante, T.A.; Paz, F.A.A.; Valente, A.A.; Gonçalves, I.S.; Pillinger, M. A Comparative Study of Molybdenum Carbonyl and Oxomolybdenum Derivatives Bearing 1,2,3-Triazole or 1,2,4-Triazole in Catalytic Olefin Epoxidation. *Molecules* **2019**, *24*, 105. [[CrossRef](#)]
48. Lysenko, A.B.; Senchyk, G.A.; Domasevitch, K.V.; Henfling, S.; Erhart, O.; Krautscheid, H.; Neves, P.; Valente, A.A.; Pillinger, M.; Gonçalves, I.S. A Molybdenum Trioxide Hybrid Decorated by 3-(1,2,4-Triazol-4-yl)adamantane-1-carboxylic acid: A Promising Reaction-Induced Self-Separating (RISS) Catalyst. *Inorg. Chem.* **2019**, *58*, 16424–16433. [[CrossRef](#)]
49. Lysenko, A.B.; Senchyk, G.A.; Domasevitch, K.V.; Neves, P.; Valente, A.A.; Pillinger, M.; Gonçalves, I.S. Hydrophobic/Hydrophilic Interplay in 1,2,4-Triazole- or Carboxylate-Based Molybdenum(VI) Oxide Hybrids: A Step Toward Development of Reaction-Induced Self-Separating Catalysts. *ChemCatChem* **2021**, *13*, 3090–3098. [[CrossRef](#)]
50. Amarante, T.R.; Neves, P.; Valente, A.A.; Paz, F.A.A.; Pillinger, M.; Gonçalves, I.S. Metal Oxide-Triazole Hybrids as Heterogeneous or Reaction-Induced Self-Separating Catalysts. *J. Catal.* **2016**, *340*, 354–367. [[CrossRef](#)]
51. Zonetti, P.C.; Celnik, J.; Letichevsky, S.; Gaspar, A.B.; Appel, L.G. Chemicals from ethanol—The dehydrogenative route of the ethyl acetate one-pot synthesis. *J. Mol. Catal. A Chem.* **2011**, *334*, 29–34. [[CrossRef](#)]
52. Martín, M.; Grossmann, I.E. On the Systematic Synthesis of Sustainable Biorefineries. *Ind. Eng. Chem. Res.* **2013**, *52*, 3044–3064. [[CrossRef](#)]
53. Mahato, N.; Sharma, K.; Sinha, M.; Baral, E.R.; Koteswararao, R.; Dhyani, A.; Cho, M.H.; Cho, S. Bio-Sorbents, Industrially Important Chemicals and Novel Materials from Citrus Processing Waste as a Sustainable and Renewable Bioresource: A Review. *J. Adv. Res.* **2020**, *23*, 61–82. [[CrossRef](#)]
54. Calhorda, M.J.; Costa, P.J. Unveiling the Mechanisms of Catalytic Oxidation Reactions Mediated by Oxo-Molybdenum Complexes: A Computational Overview. *Curr. Org. Chem.* **2012**, *16*, 65–72. [[CrossRef](#)]
55. Ucciani, E.; Debal, A.; Rafaralahitsimba, G. Epoxidation of Fatty Acid Methyl Esters with Organic Hydroperoxides and Molybdenum Oxide. *Fett/Lipid* **1993**, *95*, 236–239. [[CrossRef](#)]
56. Ucciani, E.; Bonfand, A.; Rafaralahitsimba, G.; Cecchi, G. Epoxidation of monoenic fatty esters with cumylhydroperoxide and hexacarbonylmolybdenum. *Revue Française des Corps Gras.* **1992**, *39*, 279–283.
57. Huang, Y.-B.; Yao, M.-Y.; Xin, P.-P.; Zhou, M.-C.; Yang, T.; Pan, H. Influence of Alkenyl Structures on the Epoxidation of Unsaturated Fatty Acid Methyl Esters and Vegetable Oils. *RSC Adv.* **2015**, *5*, 74783–74789. [[CrossRef](#)]
58. Tiozzo, C.; Bisio, C.; Carniato, F.; Marchese, L.; Gallo, A.; Ravasio, N.; Psaro, R.; Guidotti, M. Epoxidation with Hydrogen Peroxide of Unsaturated Fatty Acid Methyl Esters over Nb(V)-Silica Catalysts. *Eur. J. Lipid Sci. Technol.* **2013**, *115*, 86–93. [[CrossRef](#)]
59. Cecchini, M.M.; de Angelis, F.; Iacobucci, C.; Reale, S.; Crucianelli, M. Mild Catalytic Oxidations of Unsaturated Fatty Acid Methyl Esters (FAMES) by Oxovanadium Complexes. *Appl. Catal. A Gen.* **2016**, *517*, 120–128. [[CrossRef](#)]
60. Kim, N.; Li, Y.; Sun, X.S. Epoxidation of Camelina Sativa Oil and Peel Adhesion Properties. *Ind. Crops Prod.* **2015**, *64*, 1–8. [[CrossRef](#)]
61. Maiti, S.K.; Snively, W.K.; Venkitasubramanian, P.; Hagberg, E.C.; Busch, D.H.; Subramaniam, B. Reaction Engineering Studies of the Epoxidation of Fatty Acid Methyl Esters with Venturello Complex. *Ind. Eng. Chem. Res.* **2019**, *58*, 2514–2523. [[CrossRef](#)]
62. Gamelas, C.A.; Neves, P.; Gomes, A.C.; Valente, A.A.; Romão, C.C.; Gonçalves, I.S.; Pillinger, M. Molybdenum(II) Diiodo-Tricarbonyl Complexes Containing Nitrogen Donor Ligands as Catalyst Precursors for the Epoxidation of Methyl Oleate. *Catal. Lett.* **2012**, *142*, 1218–1224. [[CrossRef](#)]
63. Amarante, T.R.; Neves, P.; Valente, A.A.; Paz, F.A.A.; Fitch, A.N.; Pillinger, M.; Gonçalves, I.S. Hydrothermal Synthesis, Crystal Structure, and Catalytic Potential of a One-Dimensional Molybdenum Oxide/Bipyridinedicarboxylate Hybrid. *Inorg. Chem.* **2013**, *52*, 4618–4628. [[CrossRef](#)]
64. Deng, G.; Wang, Z. Triptycene-Based Microporous Cyanate Resins for Adsorption/Separations of Benzene/Cyclohexane and Carbon Dioxide Gas. *ACS Appl. Mater. Interfaces* **2017**, *9*, 41618–41627. [[CrossRef](#)] [[PubMed](#)]
65. Shang, Z.; Lü, C.; Zhao, J.; Yan, J.; Ding, M.; Gao, L. One-Pot Synthesis of Polyetherimides from Bis(chlorophthalimide) and Dichlorodiphenylsulfone in Diphenylsulfone. *J. Appl. Polym. Sci.* **2006**, *102*, 4584–4588. [[CrossRef](#)]
66. Wan, J.; Gan, B.; Li, C.; Molina-Aldareguia, J.; Li, Z.; Wang, X.; Wang, D.-Y. A novel biobased epoxy resin with high mechanical stiffness and low flammability: Synthesis, characterization and properties. *J. Mater. Chem. A* **2015**, *3*, 21907–21921. [[CrossRef](#)]
67. Ahn, T.-K.; Kim, M.; Choe, S. Hydrogen-Bonding Strength in the Blends of Polybenzimidazole with BTDA- and DSDA-Based Polyimides. *Macromolecules* **1997**, *30*, 3369–3374. [[CrossRef](#)]

68. Nambo, M.; Crudden, C.M. Modular Synthesis of Triarylmethanes through Palladium-Catalyzed Sequential Arylation of Methyl Phenyl Sulfone. *Angew. Chem. Int. Ed.* **2014**, *53*, 742–746. [[CrossRef](#)] [[PubMed](#)]
69. Bullock, C.X.; Jamieson, C.S.; Moënné-Loccoz, P.; Taylor, B.; Gonzalez, J.A.M.; Draves, E.A.; Kuo, L.Y. Sulfide Oxidation by 2,6-Bis[Hydroxyl(Methyl)Amino]-4-Morpholino-1,3,5-Triazinatodioxomolybdenum(VI): Mechanistic Implications with DFT Calculations for a New Class of Molybdenum(VI) Complex. *Inorg. Chem.* **2021**, *60*, 7762–7772. [[CrossRef](#)]
70. McManus, J.M.; Herbst, R.M. Tetrazole Analogs of Pyridinecarboxylic Acids. *J. Org. Chem.* **1959**, *24*, 1462–1464. [[CrossRef](#)]
71. Kottke, T.; Stalke, D. Crystal handling at low temperatures. *J. Appl. Crystallogr.* **1993**, *26*, 615–619. [[CrossRef](#)]
72. APEX3 Crystallography Software Suite, Version 2016.9-0; Bruker AXS Inc.: Delft, The Netherlands, 2005–2016.
73. Cryopad, Remote Monitoring and Control, Version 1.451; Oxford Cryosystems: Oxford, UK, 2006.
74. SAINT+ Data Integration Engine, Version 8.37A; Bruker AXS Inc.: Madison, WI, USA, 2015.
75. Krause, L.; Herbst-Irmer, R.; Sheldrick, G.M.; Stalke, D. Comparison of Silver and Molybdenum Microfocus X-Ray Sources for Single-Crystal Structure Determination. *J. Appl. Crystallogr.* **2015**, *48*, 3–10. [[CrossRef](#)]
76. Sheldrick, G.M. SHELXT—Integrated Space-Group and Crystal-Structure Determination. *Acta Crystallogr. A Found. Adv.* **2015**, *71*, 3–8. [[CrossRef](#)]
77. Sheldrick, G.M. Crystal Structure Refinement with SHELXL. *Acta Crystallogr. C Struct. Chem.* **2015**, *71*, 3–8. [[CrossRef](#)] [[PubMed](#)]
78. Hübschle, C.B.; Sheldrick, G.M.; Dittrich, B. ShelXle: A Qt Graphical User Interface for SHELXL. *J. Appl. Crystallogr.* **2011**, *44*, 1281–1284. [[CrossRef](#)] [[PubMed](#)]
79. Putz, H.; Brandenburg, K. *Diamond—Crystal and Molecular Structure Visualization*, Version 3.2f; Crystal Impact GbR: Bonn, Germany, 2010.

Disclaimer/Publisher’s Note: The statements, opinions and data contained in all publications are solely those of the individual author(s) and contributor(s) and not of MDPI and/or the editor(s). MDPI and/or the editor(s) disclaim responsibility for any injury to people or property resulting from any ideas, methods, instructions or products referred to in the content.